frontiers | Frontiers in Earth Science

TYPE Original Research
PUBLISHED 03 July 2024
DOI 10.3389/feart.2024.1428055

OPEN ACCESS

EDITED BY
Zhaochong Zhang,
China University of Geosciences, China

REVIEWED BY
William F. McDonough,
University of Maryland, United States
Junpeng Wang,
China University of Geosciences Wuhan,
China

*CORRESPONDENCE
Nijiati Abuduxun,
nijatxju@163.com

RECEIVED 05 May 2024
ACCEPTED 06 June 2024
PUBLISHED 03 July 2024

CITATION
Gong X, Abuduxun N, Jia X, Cheng Y, Cai H, Wu X and Yang H (2024), Early Jurassic A-type granite and monzodiorite from the Baoji batholith: Implication for tectonic transition from post-collision to post-orogenic extension in the Qinling Orogenic Belt, China. *Front. Earth Sci.* 12:1428055.
doi: 10.3389/feart.2024.1428055

Early Jurassic A-type granite and monzodiorite from the Baoji batholith: Implication for tectonic transition from post-collision to post-orogenic extension in the Qinling Orogenic Belt, China

Xiangkuan Gong[1], Nijiati Abuduxun[1]*, Xiaoliang Jia[2], Yuanfeng Cheng[1], Hongming Cai[1], Xueqian Wu[1] and Haodong Yang[1]

[1]Xinjiang Key Laboratory for Geodynamic Processes and Metallogenic Prognosis of the Central Asian Orogenic Belt, Department of Geology and Mining Engineering, Xinjiang University, Urumqi, China, [2]Xinjiang Research Center for Mineral Resources, Xinjiang Institute of Ecology and Geography, Chinese Academy of Sciences, Urumqi, China

Introduction: The early Jurassic granitoids in the Qinling Orogenic Belt (QOB) play a crucial role in understanding the tectonic implications for the geological evolution of China. To elucidate the early Jurassic tectonic setting of QOB, we performed a comprehensive analysis of zircon U-Pb ages, whole-rock geochemistry, and *in situ* zircon Lu-Hf isotopes from early Jurassic monzodiorite and Kfeldspar granite within the Baoji batholith in western QOB.

Geochronology Method and Results: The intrusions yielded zircon U-Pb ages of 186 ± 2 Ma and 188 ± 2 Ma, respectively.

Geochemistry Results: The monzodiorites are characterized by relatively high MgO, Rb, Th, U, and LREE contents, as well as low P, Ti, and HREE contents. They also exhibit high Nb/Ta ratios (20.6–23.4). The zircon $\varepsilon_{Hf}(t)$ values for the monzodiorite sample range from −4.36 to 6.47, indicating significant contributions from a fertile continental lithospheric mantle with the involvement of crustal components. The K-feldspar granites are enriched in K_2O+ Na_2O, Rb, Zr, Hf, and Nb, and lower Ba, Sr, Ti, and P. They exhibit high Nb/Ta and Ga/Al ratios but low Y/Nb and Yb/Ta ratios. Their geochemical characteristics reveal an A-type granite affinity with elevated zircon saturation temperatures (848°C–900 °C). Additionally, the K-feldspar granite exhibits REE and trace element patterns similar to those observed in the monzodiorite. However, a wide range of zircon $\varepsilon_{Hf}(t)$ values (−4.72 to 3.98), differing from those of the monzodiorite, indicate that the parental magma of the K-feldspar granite experienced magma mixing between a monzodioritic magma and a crustal-derived felsic magma.

Discussion: These findings suggest that both A-type K-feldspar granite and monzodiorite likely formed during post-orogenic processes. Additionally, the

QOB commenced its postorogenic evolution as an extensional tectonic environment during the early Jurassic period.

KEYWORDS

A-type granite, monzodiorite, post-orogenic extension, early Jurassic, Qinling Orogenic Belt

1 Introduction

Post-collision refers to a tectonic process characterized by crustal extension following continental collision. This results from the relaxation of compressional stresses between colliding plates, indicating the latest stage of an orogenic cycle (Liégeois, 1998; Song et al., 2015). This stage is marked by the development of extensional structures such as rifts and grabens (e.g., Buck, 1991). On the contrary, post-orogenic collapse indicates the onset of intra-plate evolution (Liégeois, 1998; Song et al., 2015), and describes the gravitational subsidence and collapse of the orogenic belt following cessation of compressional forces. This collapse is attributed to the isostatic adjustment of the lithosphere caused by erosion and sedimentation-induced removal of crustal material, resulting in basin formation (e.g., Willett et al., 1993; Dong et al., 2005). Therefore, post-collisional extension reflects lithospheric stretching and thinning, whereas intra-plate post-orogenic collapse indicates gravitational adjustment and subsidence.

The study of magmatism within continental collision zones has long been a primary focus in solid earth science research (e.g., Zhao et al., 2011; Wang et al., 2013; Song et al., 2015). Typically, A-type granites are formed in extensional settings. Therefore, they are critical for restoring the tectonic evolution of orogenic belts (Eby, 1992; Hong et al., 1996; Bonin, 2007). The Qinling Orogenic Belt (QOB) lies between the North China Block (NCB) to the north and the South China Block (SCB) to the south (Figure 1A), and plays a significant role in the continental reconstruction of China (Mattauer et al., 1985; Dong and Santosh, 2016). The QOB experienced multiple stages of accretion and collision between SCB and NCB as well as intervening microcontinents since the Proterozoic, finally leading to its formation in the Early Mesozoic (Ratschbacher et al., 2003; Wu and Zheng, 2013; Dong and Santosh, 2016). The widely exposed Triassic granitoids (ca. 250–200 Ma) in this belt reflect magmatic responses to the thermo-tectonic events associated with the convergence and collision of the two blocks. Significant advances have been made in terms of these granitoids and their mafic microgranular enclaves (MMEs) over the past few decades (e.g., Sun et al., 2002; Jin et al., 2005; Qin et al., 2005; 2008; 2009; 2010a; 2010b; Zhang et al., 2005; 2008; Gong et al., 2009a; 2009b; Dong et al., 2012; Wang et al., 2013; Xue et al., 2018). In recent times, there has been recognition of small-scale Jurassic molybdenum metallogenic events (Li et al., 2010; Zhang et al., 2015) and minor granitic intrusions (189–198 Ma, Dong et al., 2012; Xue et al., 2018; Gong et al., 2021) in the South Qinling Block (SQB) and the western segment of the North Qinling Block (NQB) (Figures 1B,C). However, the tectonic setting responsible for the formation of these granitoids and the mineralization of molybdenum remains a topic of contention. Based on petrologic, geochemical, and isotopic investigations into these granitic plutons and their morphological features, two conflicting interpretations have been proposed: 1) post-collisional extension between NCB and SCB (Wang et al., 2013; Xue et al., 2018) and 2) intra-plate post-orogenic collapse following continental collision (Li et al., 2010; Dong et al., 2012; Zhang et al., 2015).

In this study, a systematic and detailed investigation of whole-rock geochemistry, zircon U-Pb ages, and Lu-Hf isotopes of early Jurassic K-feldspar granites and monzodiorites from the Baoji batholith in QOB have been reported. Our data offers new insights into the early Jurassic tectonic evolution of QOB.

2 Geological background

The QOB is traditionally divided into NQB and SQB by the Shangdan fault (Dong and Santosh, 2016). The NQB is subdivided into four fault-bounded rock units, namely, the Kuanping Complex (KC), the Erlangping Complex (EC), the Qinling Complex (QC), and the Shangdan suture zone (SSZ) from north to south based on the rock association, isotopic geochronology, and degree of metamorphism. Voluminous early Mesozoic magmatism is well developed across all these units (Figure 1B). The KC constitutes the northernmost part of NQB. Previous investigations have revealed that KC consists of two major components: metasedimentary rocks and metabasalts. The former primarily consists of micaschists, gneisses, and minor marbles, while the latter consists of greenschists with intercalated amphibolites. Detrital zircons in the metasedimentary rocks, with the youngest magmatic ages of 530–600 Ma confirmed their deposition during the early Paleozoic (Diwu et al., 2010; Gao et al., 2015). Ophiolites and low metamorphic-grade sedimentary successions are the major units of EC (Sun et al., 1996; Dong et al., 2011). The ophiolitic unit primarily consists of basalts with minor sheeted dikes and/or sills, cherts, and marbles (Diwu et al., 2014). Wang et al. (1995) reported early to middle Ordovician radiolarians in the cherts interlayered within the basalts. High-precision SHRIMP/LA-ICP-MS zircon U-Pb chronology of the greenschist facies metasedimentary rocks (500–3,894 Ma, Yang et al., 2016), basic volcanic rocks (460–475 Ma, Yan et al., 2007; Zhao et al., 2012), and lenticular leucosomes within the volcanics (468–470 Ma, Yang et al., 2015) indicated the potential formation of the complex during the Cambrian-Ordovician. The QC has long been regarded as the oldest crystallization basement in NQB. It appears as a lenticular body between EC and SSZ and is characterized by widely distributed gneisses, schists, marbles, and amphibolites. The protoliths of these are predominantly graywackes (Diwu et al., 2014), limestones, and interlayers of continental tholeiitic lavas (Dong et al., 2011). Different types of exhumed HP-UHP metamorphic rocks with peak metamorphic ages of ca. 490–500 Ma appear as lenses

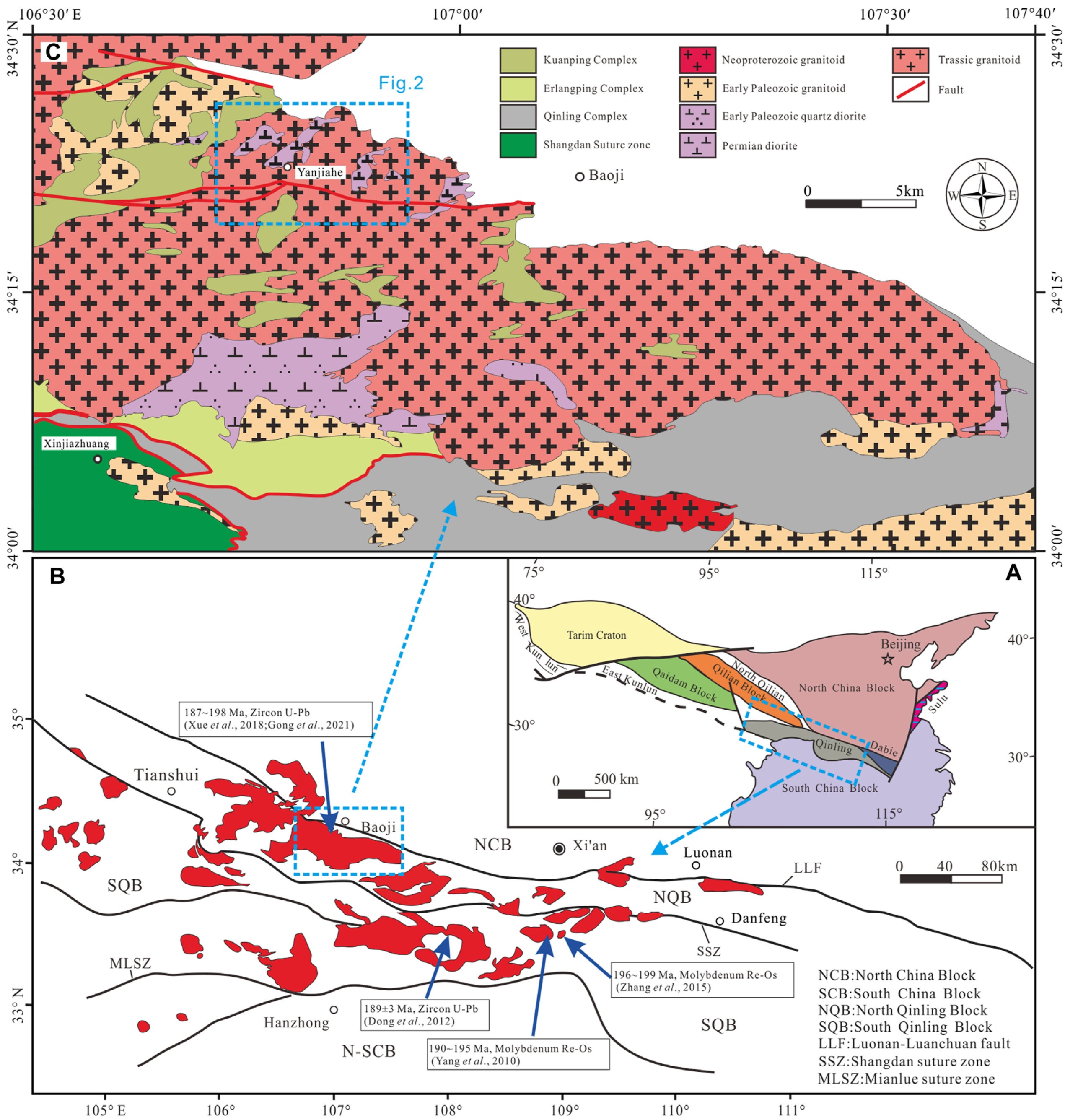

FIGURE 1
Geological sketch map of China **(A)**, geological map showing the distribution of the early Mesozoic granitoids in the QOB **(B)**, modified after Zhang et al., 2008), and geological map of the Baoji batholith **(C)**, after the 1:250,000 geological map of Baoji, Shaan' xi)

or layers within garnet-bearing paragneiss (Wang et al., 2014; Gong et al., 2016; Liu et al., 2016). They were interpreted as products of deep continental subduction between SQB and NCB along SSZ (Liu et al., 2016). Comprehensive geochronological studies of the metasedimentary rocks and Neoproterozoic granites revealed that the formation of QC can be dated back to late Mesoproterozoic to early Neoproterozoic (Diwu et al., 2014). The SSZ primarily comprises ophiolites, subduction-related volcanic rocks, and sedimentary rocks that have undergone greenschist facies metamorphism (Dong et al., 2011). Previous geochemical and geochronological data revealed that the mafic rocks in the western part of this unit, with zircon U-Pb ages of ca. 450–534 Ma, exhibit N-MORB, E-MORB, boninite, and island arc basalt fingerprints (Dong et al., 2011; Li et al., 2015).

The Baoji batholith, with a total outcrop area of approximately 1,500 km^2, occurs along SSZ within the western segment of NQB. The batholith is a composite granitic intrusion formed by multiple phases of magma emplacement and primarily comprises

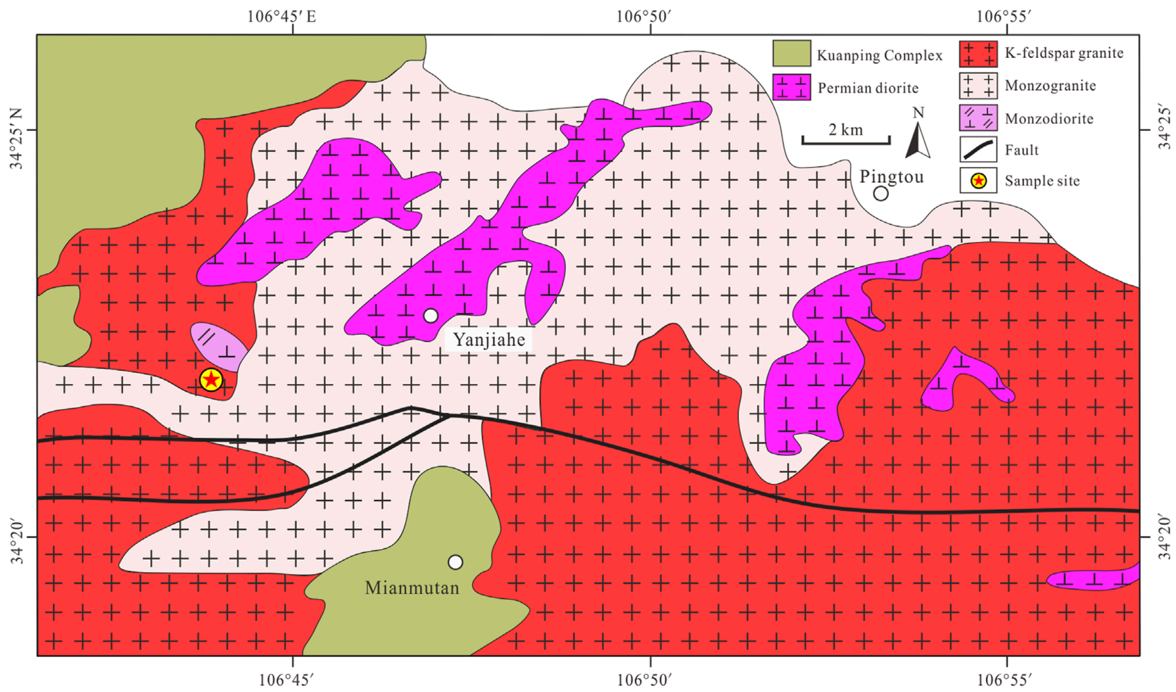

FIGURE 2
Geological map of the Baoji batholith in the Pingtou Town, Baoji City, western Shaan' xi Province (modified after 1:250,000 geological map of Baoji, Shaan' xi; Xue et al., 2018).

coarse-to medium-grained monzogranites, quartz monzonites, monzodiorites, and K-feldspar granites. It extends in an NW-SE direction and intrudes into the mica-quartz schist in KC to the north, the intermediate-acid volcanic and sedimentary rocks in EC in the middle, and the biotite plagioclase gneisses, biotite plagioclase metagranulitites, and marbles in QC to the south (Figure 1C). MMEs exhibiting ovoid or irregular shapes are abundant within the host granitoids. Generally, the MMEs exhibit an igneous texture, and contain needle-like apatite crystals, and plagioclase-mantled alkali feldspar megacrysts. They are considered to have formed by mingling and mixing processes involving the injection of mafic magma into felsic magmas (Wang et al., 2011; Xue et al., 2018).

3 Sample description

In this study, 12 representative K-feldspar granite and monzodiorite samples were collected from Yanjiahe Village (34°21′52.8″N, 106°44′20.7″E), Pingtou Town, and Baoji City (Figure 2). These consist of 6 K-feldspar granites and 6 monzodiorites. All collected samples were fresh without any subsequent alteration, deformation, or metamorphism (Figures 3A–C). Field observations revealed the intrusion of monzodiorites by K-feldspar granites (Figure 3B). A few irregular MMEs, with diameters ranging from 5 to 15 cm, were discovered within the K-feldspar granites (Figure 3C).

The K-feldspar granite is medium-to fine-grained and red in color. It is composed of K-feldspar (48–50 vol%), plagioclase (19–21 vol%), quartz (22–24 vol%), and biotite (6–8 vol%) (Figures 3D,E), with accessory minerals of sphene, zircon, and apatite. The monzodiorite exhibits a fine-grained, massive structure, and has a dark gray color. It is primarily comprised of plagioclase (53–55 vol%), K-feldspar (21–23 vol%), hornblende (13–15 vol%), biotite (6–8 vol%), and quartz (2–3 vol%), with accessory minerals of zircon, sphene, epidote, and apatite (Figure 3F).

Two samples, one from the K-feldspar granite (YJH01) and the other from the monzodiorite (YJH03), were chosen for zircon U-Pb geochronology and in *suit* Lu-Hf isotopic analysis. Additionally, six representative samples of each rock type were chosen for whole-rock geochemistry.

4 Analytical methods

All the analyses were conducted at the State Key Laboratory of Continental Dynamics, Northwest University, Xi'an, China.

4.1 Optical microscopy

Firstly, the thin sections were analyzed using a conventional binocular microscope. A Nikon LV100POL transmitted/reflected polarizing microscope, equipped with a digital camera system, was employed for petrographic observation of the textural features of the samples and examination of the primary relationships among mineral grains.

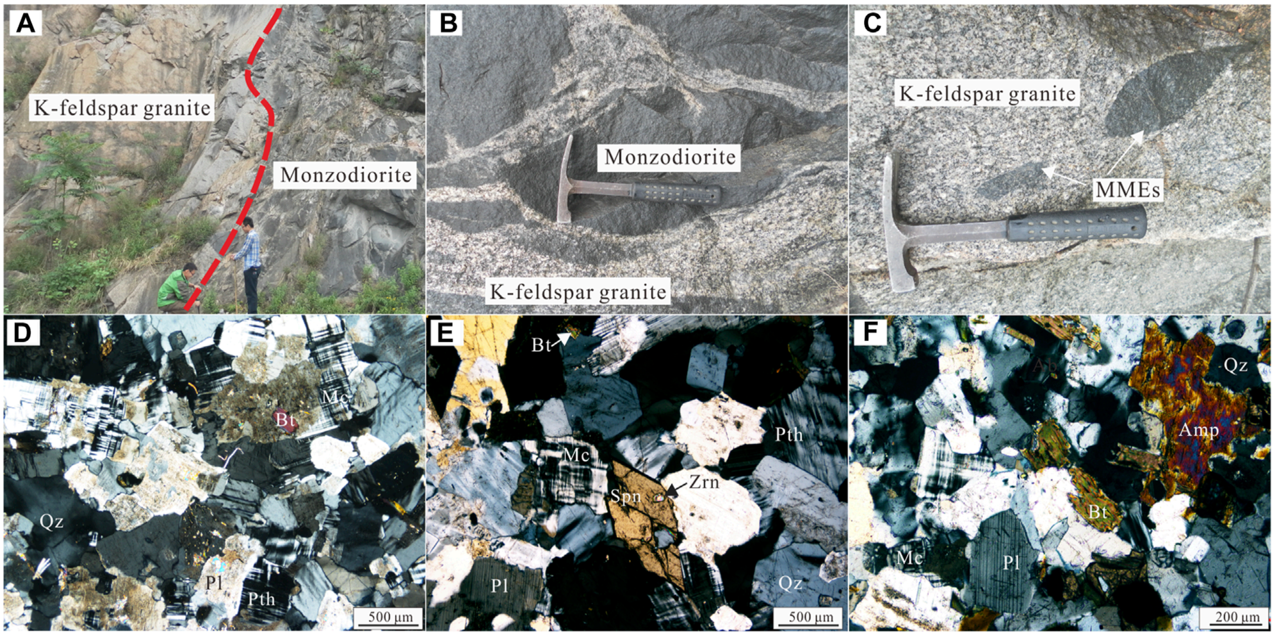

FIGURE 3
Field photographs showing the field occurrences of the K-feldspar granite and the monzodiorite **(A, B, C)**, microscopic photographs of the K-feldspar granite **(D, E)**, and the monzodiorite **(F)** from the Baoji batholith, western Qinling, China. **(A)** Outcrop photograph of the K-feldspar granite and the monzodiorite. **(B)** The monzodiorite was intruded by the K-feldspar granite. **(C)** MMEs with irregular shape occurring within K-feldspar granite. **(D)** and **(E)** Microscopic photograph shows that mineral assemblage of K-feldspar granite are Qz+Pth+Pl+Mc+Bt, and accessory minerals are mainly zrn and Spn. **(F)** Mineral assemblage of monzodiorite are Pl+Mc+Amp+Bt+Qz. Abbreviation: Mc: microcline, Pth: perthite, Pl: plagioclase, Bt: biotite, Qz: quartz, Amp: amphibole, Spn: sphene; Zrn: zircon.

4.2 LA-ICP-MS zircon U-Pb geochronology

After crushing and sieving 5–6 kg of each sample, zircon grains were separated using traditional density and magnetic separation methods. Individual zircons were handpicked and mounted in epoxy resin. The samples were polished using Al_2O_3 powders to determine their inner structure. Cathodoluminescence (CL) images were captured using a Quanta 400FEG environmental scanning electron microscope configured with a Gatan CL3+ CL detector at 20 kV.

Zircon U-Pb dating and trace elemental measurements were conducted synchronously using an Agilent 7500a ICP-MS attached to a 193 nm ArF-excimer laser ablation system. The spots had a diameter of 30 μm, and a laser repetition rate of 8 Hz was chosen. High-purity helium was used as a carrier gas. Zircon 91,500, with a $^{206}Pb/^{238}U$ age of 1,065.4 ± 0.6 Ma, was chosen as an external standard. The instrument was optimized using silicate glass NIST 610 as an external standard. U-Th-Pb isotope ratios and element concentrations were determined using Glitter 4.0. Concordia diagrams and weighted mean calculations were created using ISOPLOT/Excel version 3.6 (Ludwig, 2003).

4.3 Lu-Hf isotopic analyses

Nu Plasma II MC-ICP-MS with a RESOlution M-50 193 nm laser system was employed for *in situ* zircon Lu-Hf isotopic analyses using helium as a carrier gas. The laser repetition rate was set to 6 Hz, with an energy density of 6 J/cm^2 and a beam spot diameter of 44 μm. Additional information about these instruments, analytical approaches, and data analysis can be found in Yuan et al. (2008) and Bao et al. (2017). Data quality was assessed using the reference external calibration standards such as zircon 91,500 and mudtank. The ε_{Hf} values were derived using a decay constant value of 1.867 × 10^{-11} yr^{-1} for ^{176}Lu (Albarède et al., 2006), as well as the current chondritic ratios of $^{176}Hf/^{177}Hf = 0.282772$ and $^{176}Lu/^{177}Hf = 0.0332$ (Blichert-Toft and Albarède, 1997). $T_{DM}1$ (single-stage Hf model ages) were calculated based on the depleted mantle with a current $^{176}Hf/^{177}Hf$ ratio of 0.28325 and a $^{176}Lu/^{177}Hf$ ratio of 0.0384 (Griffin et al., 2000). To calculate $T_{DM}2$ (two-stage Hf model ages), a mean $^{176}Lu/^{177}Hf$ of 0.015 for the average continental crust (Rudnick and Gao, 2003) was assumed.

4.4 Whole-rock geochemistry

Major elements of whole-rock were analyzed using an XRF spectrometer (Rigaku RIX 2100) with Li-borate glass beads. Based on the analyses of international (USGS) rock standards BHVO-1 and AGV-1, precision and accuracy exceeded 95%.

Agilent 7500a ICP-MS was used to analyze trace elements following the acid digestion of sample powders in Teflon bombs. The instrument was calibrated using international standards BHVO-2, AGV-2, BCR-2, and GSP-2. Analytical accuracy exceeded 95% for Co, Ni, Zn, Ga, Rb, Y, Zr, Nb, Hf, Ta, and REEs, and 90%–95% for others.

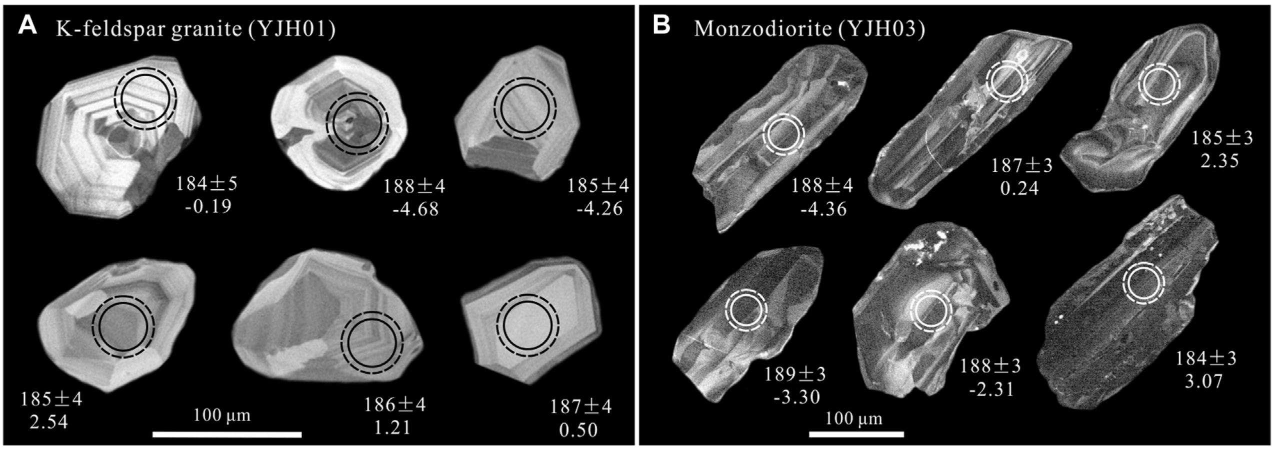

FIGURE 4
Cathodoluminescence (CL) images of representative zircons from the K-feldspar granite **(A)** and the monzodiorite **(B)**, western Qinling, China. Solid circles indicate positions of dated laser spots, dashed circles indicate positions of Lu-Hf analyses. Corresponding ages and $\varepsilon_{Hf}(t)$ values are also marked.

5 Results

5.1 Zircon U-Pb dating and trace elements

The LA-ICP-MS zircon U-Pb data for the K-feldspar granite (YJH01) and monzodiorite (YJH03) are provided in Supplementary Table S1.

All zircons from the Yanjiahe K-feldspar granite YJH01 exhibit colorless, transparent, euhedral to subhedral granular or short columnar crystals with well-defined oscillatory zones (Figure 4A). The length of the crystals varies from 80 to 120 μm, exhibiting aspect ratios between 1:1 and 1.3:1. A total of twenty-one analyses on 21 zircons were conducted for the sample YJH01. Zircons have moderate Th (73×10^{-6} to 521×10^{-6}) and U (58×10^{-6} to 332×10^{-6}) contents, with high Th/U ratios of 1.10–2.60. The chondrite-normalized rare earth element (REE) patterns of the dated zircons reveal a magmatic origin (Figure 5A). These spots yield concordant $^{206}Pb/^{238}U$ ages between 183 and 191 Ma, defining a weighted average age of 188 ± 2 Ma (MSWD = 0.26). This age is regarded as the crystallization age of the K-feldspar granite (Figure 5B).

Zircons from the Yanjiahe monzodiorite YJH03 are colorless to faint yellow transparent crystals. Most grains exhibit long columnar or short columnar crystals (180–300 μm in length with an aspect ratio between 2:1 and 3:1) (Figure 4B). Most zircons exhibit magmatic cores and dark rims (Figure 3B), indicating that they underwent subsequent dissolution and regeneration in a fluid-rich environment following crystallization. The rims of the zircons demonstrate a narrow width. Therefore, twenty-two spots on the cores of 22 zircons from this sample were analyzed (Supplementary Table S1). All zircons exhibit significantly high Th (240×10^{-6} to 1870×10^{-6}) and U (185×10^{-6} to $1{,}098 \times 10^{-6}$) contents, with Th/U ratios between 0.45 and 3.77. The chondrite-normalized REE patterns exhibit a steep positive slope, strong Ce positive anomalies, and pronounced Eu negative anomalies, indicating a magmatic origin (Figure 5C). The concordant $^{206}Pb/^{238}U$ ages of these analytical spots range from 180 to 191 Ma and yield a weighted average age of 186 ± 2 Ma (MSWD = 0.57) (Figure 5D), indicating the crystallization age of the monzodiorite.

5.2 Zircon Lu-Hf isotopes

In situ zircon Lu-Hf isotopic data for the samples are listed in Supplementary Table S2 and graphically represented in Figure 6. The $\varepsilon_{Hf}(t)$ and T_{DM} values were calculated based on their apparent $^{206}Pb/^{238}U$ ages.

Twenty-one zircons dated from the K-feldspar granite exhibit a range of $^{176}Lu/^{177}Hf$ (0.000943–0.002030) and $^{176}Hf/^{177}Hf$ (0.282527–0.282773) ratios, with $\varepsilon_{Hf}(t)$ values ranging from −4.72 to 3.98. Among the 21 analyses conducted, nine exhibit positive $\varepsilon_{Hf}(t)$ values between 0.05 and 3.98, with corresponding single-stage Hf model ages ranging from 0.69 to 0.85 Ga. The remaining 12 analyses exhibit negative $\varepsilon_{Hf}(t)$ values between −0.15 and −4.72, with corresponding two-stage Hf model ages ranging from 1.24 to 1.52 Ga.

Twenty-two analyses from the monzodiorite sample exhibit a wide variation in the Hf isotopic compositions. Fourteen spots exhibit negative $\varepsilon_{Hf}(t)$ values ranging from −1.57 to −4.36, with corresponding two-stage Hf model ages ranging from 1.32 to 1.50 Ga. The other remaining 8 spots exhibit positive $\varepsilon_{Hf}(t)$ values ranging from 0.24 to 6.47. Their single-stage Hf model ages vary from 0.59 to 0.83 Ga.

5.3 Whole-rock major and trace elements

The whole-rock major and trace element geochemical analytical results of twelve representative samples are provided in Table 1. Samples from the K-feldspar granite exhibit a limited range of chemical compositions, characterized by high contents of SiO_2 (68.30–71.22 wt%), K_2O (4.99–6.23 wt%), and Na_2O (4.22–4.59 wt%). These samples also exhibit variable K_2O/Na_2O ratios (1.12–1.38) and form a shoshonitic series with

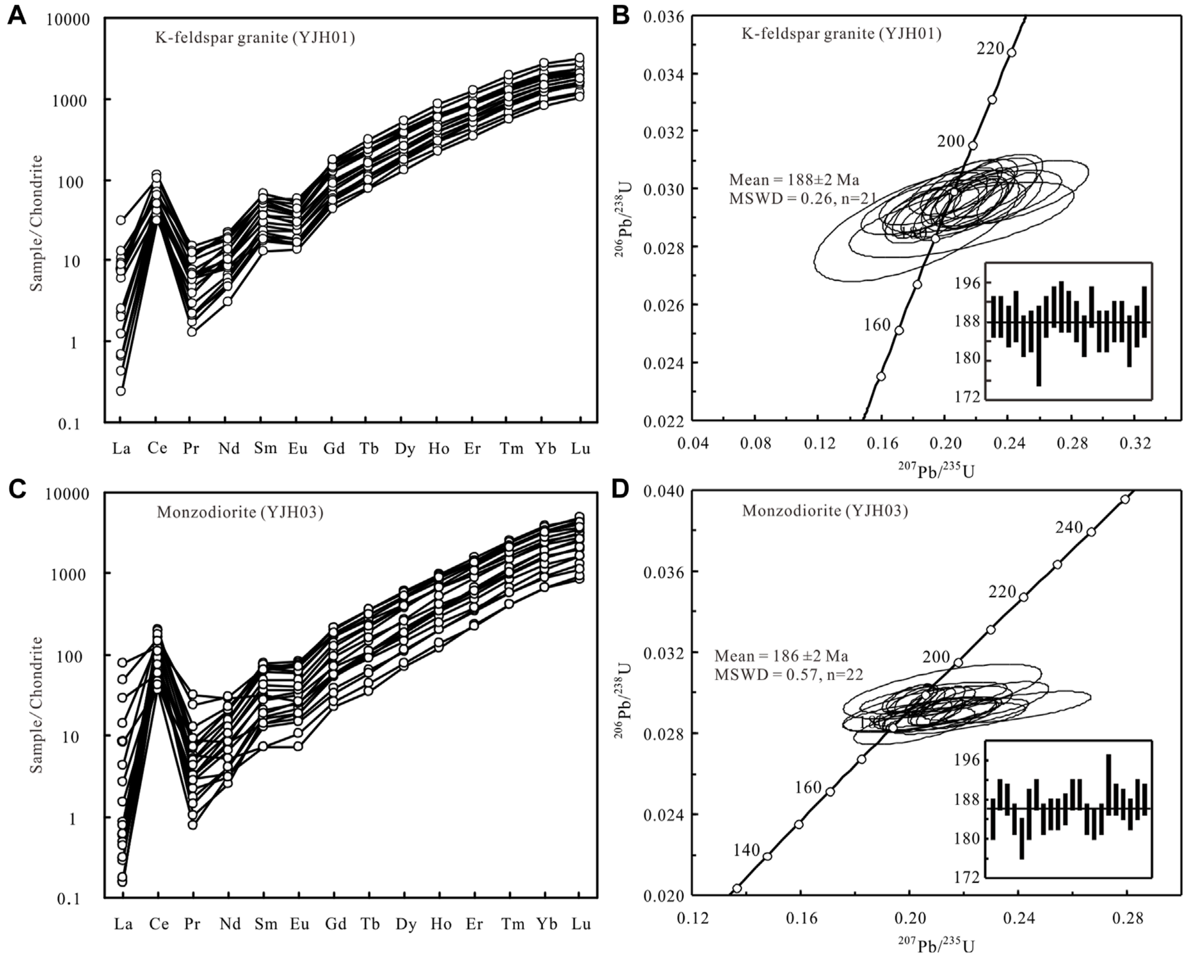

FIGURE 5
Concordia diagrams of zircon U-Pb ages and chondrite-normalized REE patterns of the K-feldspar granite **(A, B)** and monzodiorite **(C, D)**. Chondrite-normalization values are from Sun and McDonough, 1989.

combined Na_2O+ K_2O contents ranging from 9.42 to 10.82 wt% (Figure 7B). On the contrary, these samples exhibit low CaO (0.67–1.40 wt%), $Fe_2O_3^T$ (1.48–2.57 wt%), MgO (0.32–0.59 wt%), and TiO_2 (0.20–0.42 wt%) contents, with low Mg# (Mg# = $Mg^{2+}/(Mg^{2+}+Fe^{2+})$) values ranging from 30.6 to 36.0. The A/CNK ratios, varying between 0.97 and 1.03, demonstrate a spectrum from metaluminous to weakly peraluminous (Figure 7A). Based on the primitive mantle-normalized trace element diagrams, all samples are significantly enriched in light rare earth elements (LREEs; $(La/Yb)_N$ = 16.3–34.9), large-ion lithophile elements (LILEs; Rb, Th, and U), and certain high-field strength elements (HFSEs; Nb and Zr), but deficient in Ba, Sr, Ti, and P (Figure 8A). They exhibit moderate total REEs of 188 × 10^{-6} to 406 × 10^{-6}, with strong negative Eu anomalies (δEu = 0.55–0.72) and nearly flat HREE patterns, as shown in Figure 8B.

Compared to K-feldspar granites, samples from the monzodiorite exhibit intermediate contents of SiO_2 (55.16–56.92 wt%) and K_2O (4.39–4.56 wt%) and high contents of Al_2O_3 (16.69–17.11 wt%), $Fe_2O_3^T$ (6.58–7.13 wt%), MgO (2.72–3.05 wt%), CaO (4.17–4.47 wt%), and Na_2O (4.80–4.90 wt%), with relatively high Mg# values (49.1–49.9) and low K_2O/Na_2O ratios (0.90–0.94). All samples exhibit a shoshonitic affinity and are classified as metaluminous rocks (Figure 7) with A/CNK values of 0.81–0.82. The primitive mantle-normalized trace element diagrams demonstrate enrichment of Rb, Th, and U but depletion of P and Ti in monzodiorites (Figure 8A). The chondrite-normalized REE patterns (Figure 8B) are characterized by a steep negative slope from La to Lu, with slight Eu anomalies (δEu = 0.88–0.91) and high $(La/Yb)_N$ ratios of 27.8–29.9.

5.4 Zircon saturation temperatures

The zircon saturation temperatures of the Yanjiahe K-feldspar granite were determined from its whole-rock composition using the zircon saturation thermometry method proposed by Watson and Harrison (1983). The calculated parameter *M* values (*M* = (Na + K + 2 × Ca)/(Si + Al)) ranged from 1.36 to 1.55, which are consistent with the recommended range (0.9–1.7). The K-feldspar granite exhibits high Zr contents of 320 × 10^{-6}–511 × 10^{-6}, with an average content of 430 × 10^{-6}. This defines a formation temperature between 848°C and 900 °C (Table 1), indicating granitic magma

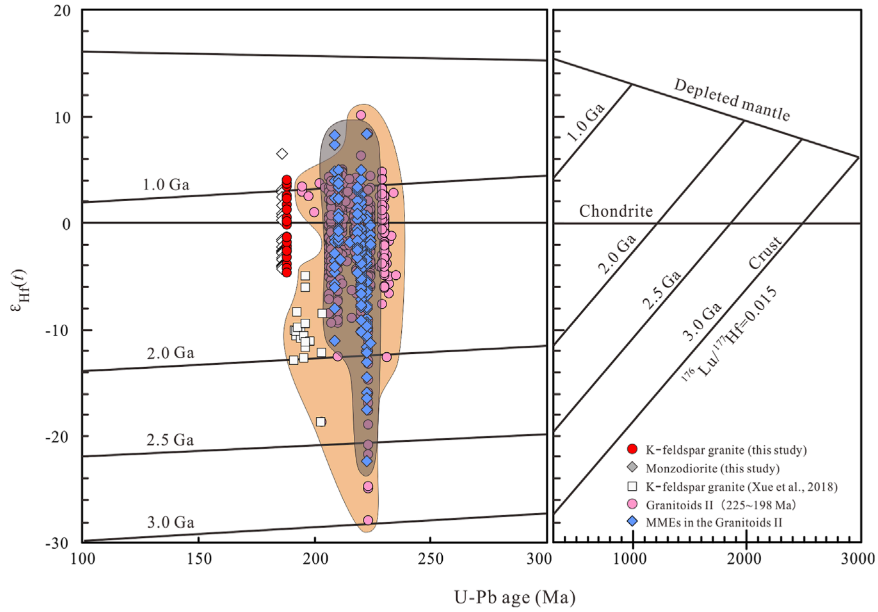

FIGURE 6
Zircon Hf isotopic compositions of the Yanjiahe K-feldspar granite and monzodiorite. The data of the granite II are after Gong et al., 2009a, Gong et al., 2009b; Qin et al., 2009, Qin et al., 2010a, Qin et al., 2010b; Li et al., 2012; Xue et al., 2018. The data of MMEs in the Granitoids II are after Gong et al., 2009b; Qin et al., 2009, Qin et al., 2010a, Qin et al., 2010b; Gong et al., 2021.

formation at a high temperature. The calculated parameter *M* values of the monzodiorites (2.55–2.68) are higher than the recommended range, and their zircon saturation temperatures were not calculated in this study.

6 Discussion

6.1 Identification of A-type granites in the Baoji batholith

A-type granites have commonly been considered a unique type of granite for more than 40 years (Loiselle and Wones, 1979). Geochemically, A-type granites typically exhibit high K_2O + Na_2O contents and Ga/Al ratios. They are further characterized by K, Ga, Rb, U, and Th enrichments, as well as Ca, Sr, Ba, Ti, and P depletions. REEs (except Eu) and some high field strength elements (HFSEs), such as Zr, Hf, and Nb, are generally high in A-type granites (e.g., Whalen et al., 1987; Eby, 1990; Bonin, 2007). Several studies have demonstrated that A-type granites can be compositionally diversified into peralkaline granites containing alkali mafic minerals (e.g., arfvedsonite, riebeckite, and sodic pyroxene), or metaluminous to weak peraluminous granites containing biotite and amphibole (e.g., Qiu et al., 2000; Wu et al., 2002; Shellnutt and Zhou, 2007). Generally, it is also widely accepted that A-type granites are generated from high-temperature magmas (Clemens et al., 1986; Patiño Douce, 1997; Zhang et al., 2012).

The distinction between A-type granites and fractionated granites is challenging (Wu et al., 2007). Xue et al. (2018) suggested that the K-feldspar granites from the Baoji batholith with zircon U-Pb ages of 194–198 Ma exhibit geochemical fingerprints of both fractionated granites and A-type granites. Gong et al. (2021) proposed that the biotite granites from the early Jurassic geochemically exhibit an A-type granite affinity. However, a lack of systematic geological data makes it uncertain whether other Jurassic granitoids from the batholith can be classified as A-type granites. The Yanjiahe K-feldspar granite samples are characterized by their metaluminous to weak peraluminous compositions and contain biotite. All samples exhibit high levels of K_2O + Na_2O and ΣREE, along with Rb, Th, U, Nb, and Zr enrichments. On the contrary, they exhibit low CaO contents and depleted Sr, Ba, Ti, and P (Table 1). All these features indicate an A-type granite affinity. Furthermore, most of these samples exhibit high Ga/Al × 10,000 ratios exceeding 2.56, which is one of the major features of A-type granites. In the discrimination diagrams plotting K_2O + Na_2O and Zr *versus* Ga/Al × 10,000, (K_2O + Na_2O)/CaO, and Ga/Al × 10,000 *versus* Zr + Nb + Ce + Y discrimination diagrams, all samples from the K-feldspar granite are within the field of A-type granite (Figure 9). The zircon saturation temperatures for the analyzed samples vary between 848 °C and 900 °C, with an average temperature of 874 °C. This is significantly higher than that of typical I-type granites (e.g., Zhao et al., 2008). Although no inherited zircons are observed in CL images (Figure 10), both Zr contents and *T*zr of the samples decrease with increasing SiO_2 content, indicating oversaturation of Zr in the granitic melt during continuous fractional crystallization processes (Chappell et al., 2000; Chappell et al., 2004). Therefore, the calculated temperatures based on sample compositions can effectively indicate the magma formation temperature. These pieces of evidence strongly indicate that the early Jurassic K-feldspar granite from the Baoji batholith belongs to 'hot' A-type granites.

10.3389/feart.2024.1428055

TABLE 1 Major (wt%) and trace ($\times 10^{-6}$) elemental compositions of the studied samples.

Sample	K-feldspar granite						Monzodiorite					
	YJH1-1	YJH1-2	YJH1-3	YJH1-4	YJH1-5	YJH1-6	YJH3-1	YJH3-2	YJH3-3	YJH3-4	YJH3-5	YJH3-6
SiO_2	71.22	68.52	68.30	69.59	69.66	69.85	55.37	56.92	55.27	55.16	56.86	55.55
TiO_2	0.20	0.33	0.34	0.42	0.42	0.38	1.29	1.21	1.32	1.28	1.24	1.32
Al_2O_3	14.63	15.90	15.85	14.87	14.88	15.18	16.95	16.81	17.11	16.96	16.69	17.03
$Fe_2O_3^T$	1.48	2.28	2.33	2.46	2.44	2.57	7.13	6.58	7.10	6.93	6.73	6.99
MnO	0.03	0.06	0.06	0.04	0.04	0.06	0.13	0.12	0.12	0.12	0.12	0.12
MgO	0.32	0.45	0.44	0.57	0.59	0.51	3.05	2.72	3.04	2.94	2.83	2.90
CaO	0.91	0.67	0.67	1.40	1.39	1.08	4.47	4.20	4.47	4.42	4.17	4.43
Na_2O	4.22	4.58	4.59	4.48	4.43	4.41	4.84	4.83	4.89	4.80	4.86	4.90
K_2O	5.81	6.19	6.23	5.00	4.99	5.59	4.50	4.54	4.42	4.53	4.39	4.56
P_2O_5	0.12	0.10	0.10	0.14	0.14	0.13	0.98	0.90	1.00	0.95	0.91	0.97
LOI	0.62	0.53	0.63	0.64	0.66	0.59	0.90	0.75	0.84	2.30	1.38	0.76
Total	99.56	99.61	99.54	99.61	99.64	100.35	99.61	99.58	99.58	100.39	100.18	99.53
FeO^T	1.33	2.05	2.10	2.21	2.20	2.31	6.42	5.92	6.39	6.24	6.06	6.29
K_2O+Na_2O	10.03	10.77	10.82	9.48	9.42	10.00	9.34	9.37	9.31	9.33	9.25	9.46
K_2O/Na_2O	1.38	1.35	1.36	1.12	1.13	1.27	0.93	0.94	0.90	0.94	0.90	0.93
Mg#	34	32	31	35	36	32	50	49	50	50	50	49
Sc	2.19	4.02	3.92	2.39	2.40	3.92	10.9	10.6	11.2	11.1	10.6	11.4
V	11.1	20.2	20.2	29.1	29.3	19.9	110	101	110	109	104	111
Cr	3.16	4.00	2.70	4.45	9.16	3.04	11.5	9.41	10.0	10.4	10.4	9.52
Co	141	140	114	146	147	128	54.9	60.1	56.2	47.1	59.5	44.3
Ga	20.4	22.5	22.0	20.1	21.1	21.3	20.9	20.3	20.7	20.6	20.9	20.6

(Continued on the following page)

TABLE 1 (*Continued*) Major (wt%) and trace (×10^{-6}) elemental compositions of the studied samples.

Sample	K-feldspar granite						Monzodiorite					
	YJH1-1	YJH1-2	YJH1-3	YJH1-4	YJH1-5	YJH1-6	YJH3-1	YJH3-2	YJH3-3	YJH3-4	YJH3-5	YJH3-6
Rb	171	195	199	109	109	173	154	148	149	147	157	144
Sr	344	357	351	733	724	338	1,448	1,369	1,461	1,462	1,351	1,479
Y	18.1	28.7	28.8	21.1	21.2	32.0	32.8	31.0	32.2	31.7	30.4	33.0
Zr	321	481	512	432	429	410	373	384	401	405	392	478
Nb	58.9	116	116	45.4	45.8	115	60.7	62.4	61.4	60.2	62.7	61.5
Cs	2.01	2.16	2.15	1.06	1.06	2.24	2.86	2.41	2.63	2.31	2.69	2.32
Ba	1,071	1,067	1,123	1,590	1,586	922	2,237	2,226	2,195	2,255	2091	2,312
La	49.5	104	107	108	108	118	114	111	115	110	107	112
Ce	86.1	168	171	163	162	186	200	191	201	195	188	201
Pr	8.61	16.3	17.1	15.6	15.6	18.3	21.8	20.5	21.7	21.1	20.2	21.9
Nd	27.4	49.4	51.2	47.2	47.1	54.5	74.7	70.0	74.2	72.5	68.8	75.2
Sm	4.17	7.12	7.22	6.32	6.42	7.69	10.9	10.2	10.8	10.6	9.97	11.0
Eu	0.90	1.19	1.20	1.37	1.36	1.31	2.84	2.72	2.87	2.81	2.67	2.97
Gd	3.49	6.01	6.11	5.42	5.49	6.57	8.94	8.42	8.90	8.73	8.25	9.05
Tb	0.49	0.80	0.82	0.65	0.66	0.87	1.08	1.02	1.07	1.06	1.01	1.11
Dy	2.91	4.70	4.85	3.67	3.65	5.22	5.87	5.52	5.84	5.72	5.42	5.97
Ho	0.59	0.93	0.96	0.68	0.69	1.02	1.09	1.02	1.07	1.05	1.00	1.10
Er	1.87	2.93	2.99	2.06	2.05	3.11	3.07	2.88	2.98	2.97	2.85	3.09
Tm	0.31	0.48	0.48	0.32	0.32	0.49	0.43	0.40	0.42	0.41	0.39	0.43
Yb	2.17	3.31	3.39	2.24	2.22	3.37	2.88	2.66	2.77	2.69	2.61	2.89

(Continued on the following page)

10.3389/feart.2024.1428055

TABLE 1 (*Continued*) Major (wt%) and trace ($\times 10^{-6}$) elemental compositions of the studied samples.

Sample	K-feldspar granite						Monzodiorite					
	YJH1-1	YJH1-2	YJH1-3	YJH1-4	YJH1-5	YJH1-6	YJH3-1	YJH3-2	YJH3-3	YJH3-4	YJH3-5	YJH3-6
Lu	0.36	0.52	0.53	0.36	0.36	0.51	0.44	0.41	0.42	0.41	0.40	0.44
Hf	8.28	11.9	12.3	10.2	10.0	9.48	7.21	7.73	7.84	8.07	7.99	9.41
Ta	3.56	6.92	7.27	2.46	2.46	6.37	2.95	2.93	2.70	2.57	2.93	2.70
Pb	46.7	48.4	46.6	30.1	29.8	44.6	26.9	27.4	26.2	27.0	26.5	27.0
Th	48.1	52.0	53.2	74.2	74.4	46.8	18.5	20.7	19.9	18.9	22.1	19.1
U	6.08	12.2	9.47	6.46	6.39	10.5	4.33	5.64	4.47	4.45	6.47	4.52
REE	189	365	375	357	357	406	447	427	450	435	419	449
10,000 × Ga/Al	2.63	2.67	2.62	2.56	2.69	2.65	2.33	2.29	2.29	2.30	2.36	2.29
Zr+Nb+Ce+Y	484	793	827	661	659	743	666	668	696	692	673	774
Nb/Ta	16.5	16.7	15.9	18.5	18.6	18.0	20.6	21.3	22.7	23.4	21.4	22.8
δEu	0.72	0.56	0.55	0.71	0.70	0.56	0.88	0.90	0.90	0.90	0.90	0.91
$(La/Yb)_N$	16.3	22.4	22.7	34.6	34.9	25.0	28.3	29.8	29.9	29.3	29.5	27.8
$(Gd/Yb)_N$	1.33	1.50	1.49	2.00	2.04	1.61	2.56	2.62	2.66	2.69	2.61	2.59
T_{zr}	848	894	900	867	867	869						

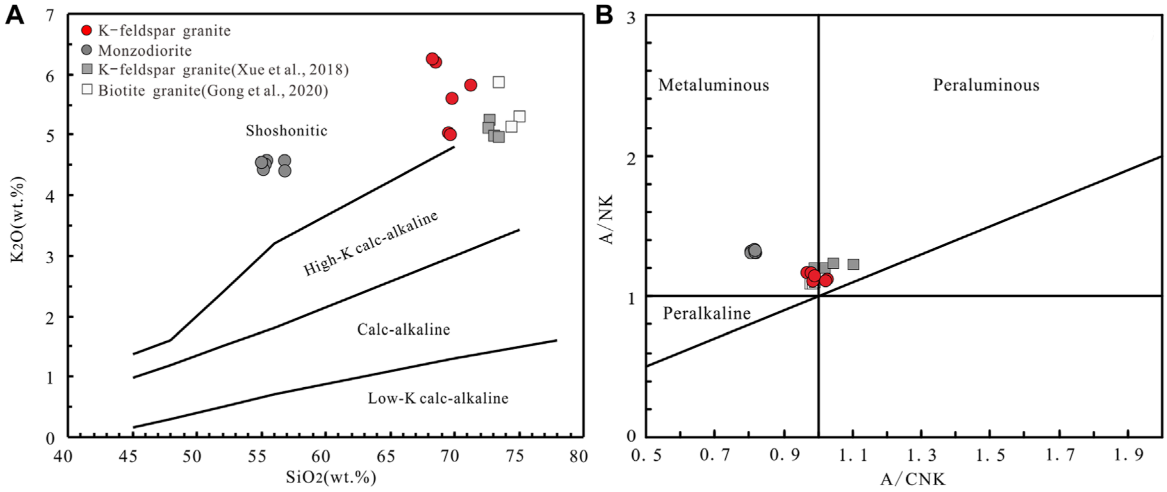

FIGURE 7
Plots of **(A)** K_2O *versus* SiO_2 (after Rollinson, 1993) and **(B)** A/NK (molar $Al_2O_3/(Na_2O+K_2O)$) *versus* A/CNK (molar $Al_2O_3/(CaO+Na_2O+K_2O)$) (after Maniar and Piccoli, 1989).

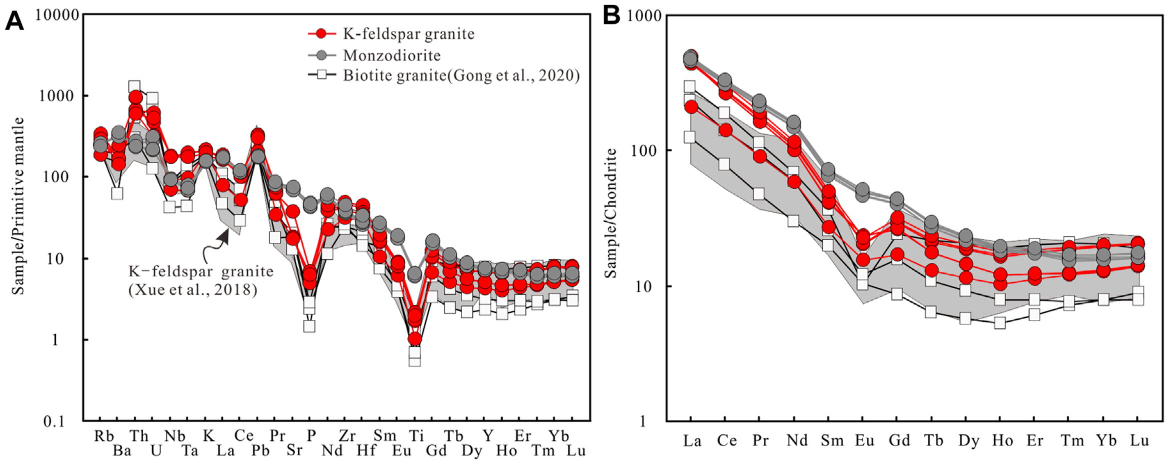

FIGURE 8
Primitive mantle-normalized spider diagrams **(A)** and chondrite-normalized REE patterns **(B)** of the K-feldspar granite and monzodiorite. The primitive mantle values are from McDonough and Sun, 1995. Chondrite values are from Sun and McDonough, 1989.

6.2 Magma sources and petrogenesis

Generally, experimental melts obtained through partial melting of metabasic crustal rocks exhibit high SiO_2 contents (>55 wt%) and low Mg# values (<44) (Beard and Lofgren, 1991; Rapp and Watson, 1995). The Yanjiahe monzodiorite samples demonstrate SiO_2 contents ranging from 55.27 to 56.92 wt% and Mg# values of 49–50, indicating their unlikely formation from crustal melts. Trace elements such as Nb and Ta are critical indicators for the distinction between crust-derived rocks and those derived from mantle magmas, as well as tracking contamination of mantle-derived rocks using crustal assimilation (Ahmed et al., 2018). Typically, igneous rocks produced by the partial melting of crustal materials exhibit significant depletion in Nb and Ta compared to mantle-derived rocks (Niu and O' Hara, 2009). The monzodiorite samples exhibit slightly negative anomalies in Nb and Ta, which do not indicate a simple crustal origin. Instead, the Nb/Ta ratios (20.6–23.4) of the monzodiorites exceed those of chondrite and primitive mantle (17.5 ± 2; Hofmann, 1988; Green, 1995). This is consistent with low degrees of partial melting in a continental lithospheric mantle produced by melt-dominated metamorphism (Aulbach et al., 2008; Yuan et al., 2010). Their shoshonitic affinity is also consistent with experimental melts generated by metasomatized mantle melting (Conceição and Green, 2004). Additionally, the samples exhibit enrichment in LILEs, LREEs, and HFSEs (Figure 8). Previous studies have revealed easy mobilization of LILEs during fluid-rock interactions, while both LREEs and HFSEs are transported by melts (Pearce and Peate, 1995; Elliott et al., 1997). Therefore, the enrichments in LILEs, LREEs, and HFSEs could be interpreted as a result of partial melting of an ancient mantle enriched by

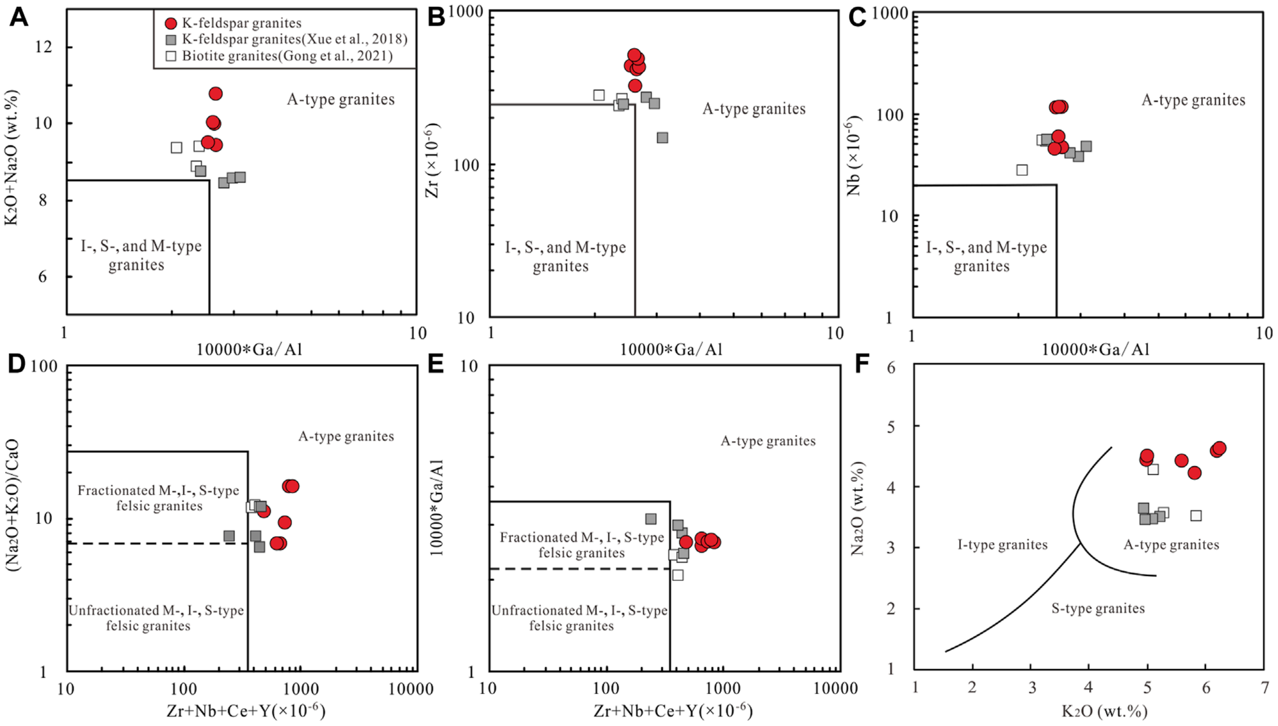

FIGURE 9
Discrimination diagrams for the Yanjiahe K-feldspar granite (**(A–E)** after Whalen et al., 1987; **(F)** after Collins et al., 1982).

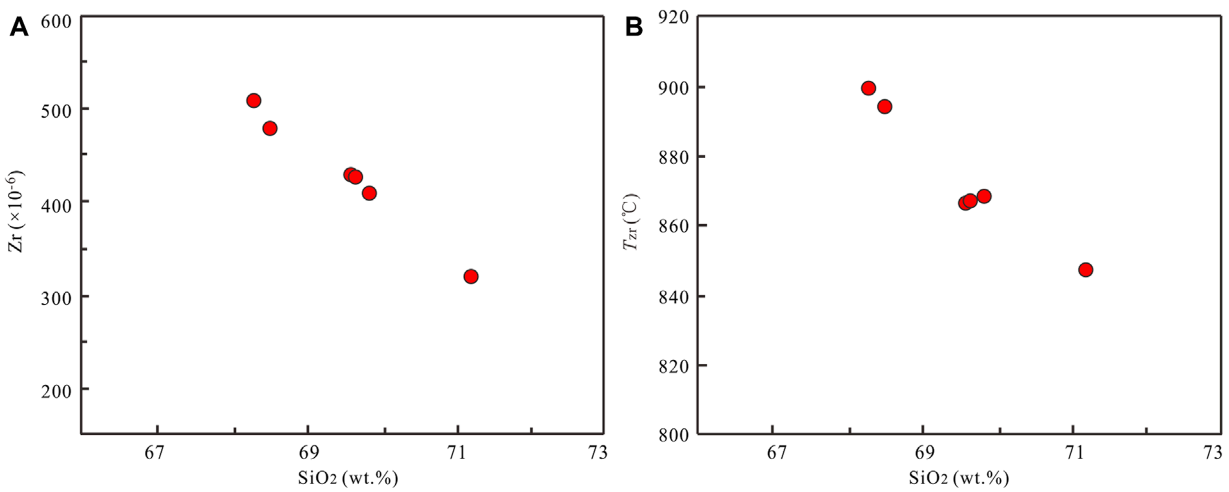

FIGURE 10
Diagrams of Zr *versus* SiO_2 **(A)** and T_{zr} *versus* SiO_2 **(B)** for the Yanjiahe K-feldspar granite.

fluids and melts. Zircons from the monzodiorite samples exhibit variable $\varepsilon_{Hf}(t)$ values ranging from −4.36 to 6.47. These values are similar to zircons from MMEs in granitoids derived from the enriched mantle (Figure 6). However, this variation in zircon $\varepsilon_{Hf}(t)$ values typically indicates the mixing of crustal and mantle-derived magmas (Shaw and Flood, 2009), or crustal assimilation of mantle-derived melt (Qin et al., 2009). Consequently, it is proposed that the monzodiorite likely originated from a fertile continental lithospheric mantle and experienced magma mixing or crustal assimilation during magma emplacement.

Previous studies have demonstrated that the early Jurassic granites from the Baoji batholith originated from the partial melting of ancient continental crust (Xue et al., 2018; Gong et al., 2021). However, the Hf isotopic compositions of the Yanjiahe K-feldspar granite are different from that of those granites (Figure 6), indicating that they likely originated from different magma sources or experienced different processes of magma evolution. Several petrogenetic models, including 1) fractional crystallization of mantle-derived magmas with or without contamination of crustal materials (Eby, 1992; Bonin, 2007), 2) partial melting of sialic crustal rocks at high temperatures (King et al., 1997; Patiño Douce, 1997; Wu et al., 2007), and 3) mixing between mantle- and crustal-derived magmas (Yang et al., 2006), have been proposed to explain the origin of A-type granites.

Figure 3B shows the intrusion of the Yanjiahe K-feldspar granite into the contemporaneous monzodiorite. These rocks exhibit similar geochemical features, such as shoshonitic affinity and enrichments in LILEs, LREEs, and HFSEs (Figure 8). However, compared to monzodiorites, the K-feldspar granites exhibit lower Al_2O_3, $Fe_2O_3{}^T$, MgO, TiO_2, CaO, Na_2O contents, and Mg# values, while presenting higher SiO_2 and K_2O contents (Figures 11A–G). These differences reveal that the two magmatic systems represented by monzodiorite and K-feldspar granite probably originated from different sources with sufficient interaction, or experienced different degrees of crustal contamination or fractional crystallization processes (Wang et al., 2011). High Nb/Ta ratios (15.9–18.6, with an average value of 17.4) observed in the K-feldspar granites are similar to those observed in mantle-derived rocks (Hofmann, 1988; Green, 1995). Additionally, their high zircon saturation temperatures are consistent with those of rocks derived from mantle sources (Ahmed et al., 2018). In terms of variations in major oxides, K-feldspar granite, and monzodiorite exhibit a uniform decrease in Al_2O_3, MgO, $Fe_2O_3{}^T$, TiO_2, MnO, and Na_2O concentrations relative to SiO_2 (Figures 11A–F). These variations can be attributed to magmatic fractional crystallization (Frost and Frost, 1997). However, the K-feldspar granites exhibit SiO_2 content exceeding 68 wt%, resulting in a silica gap between the monzodiorites and K-feldspar granites. These distinct characteristics deviate significantly from the magmatic assemblage resulting from fractional crystallization of the same magma source and can be attributed to a magma mixing process (Wang et al., 2011). Moreover, the Nb/Ta ratios of the Yanjiahe K-feldspar granite are within the range observed in both monzodiorites and early Jurassic granites from the Baoji batholith (Figure 11H), and exhibit characteristics of magma mixing (Figure 11I). The variable zircon $\varepsilon_{Hf}(t)$ values (−4.72 to 3.98) in the K-feldspar granite can also be attributed to a hybridization process involving two distinct magmas; namely, Yanjiahe monzodiorite ($\varepsilon_{Hf}(t)$ = −4.36–6.47) and early Jurassic granite ($\varepsilon_{Hf}(t)$ = −18.8 to −5.1, Xue et al., 2018). Based on these factors, along with the presence of MMEs (Figure 3C), we propose that the K-feldspar has a hybrid origin.

6.3 Constraints on tectonic setting

Over the past several years, previous studies have documented early Jurassic granitic intrusions (189–198 Ma, Figure 1B) and coeval mineralization of molybdenum (190–200 Ma, Li et al., 2010; Zhang et al., 2015) in QOB. Dong et al. (2012) proposed that the granodiorites, with a formation age of 189 ±3 Ma in SQB, probably formed in a post-orogenic extensional setting. Conversely, the granites with zircon U-Pb ages of 195–198 Ma from the Baoji batholith are considered to be products of late-collisional magmatism (Xue et al., 2018). Wang et al. (2013) also suggested that these late Triassic-early Jurassic granitoids in QOB formed in a post-collisional setting. Accordingly, the corresponding metallogenic events can be considered to be the products of magmatic-hydrothermal processes induced by intra-plate orogenic collapse (Li et al., 2010; Zhang et al., 2015). Thus, the early Jurassic tectonic regime of QOB remains a topic of contention.

Typically, A-type granites are related to extensional events; therefore, considered to be significant geodynamic indicators (Eby, 1992; Hong et al., 1996; Bonin, 2007; Song et al., 2021; Zhang et al., 2023). Hong et al. (1996) divided A-type granites into AA (anorogenic) and PA (post-orogenic) types. The first type exhibits a wide variation in R_1 values, i.e., between 500 and 3,000 (R_1 = 4Si - 11(Na + K) - 2(Fe + Ti)), with high Ga/Al × 10,000 ratios of 4–9. In the second type, R_1 values fall within a narrow range of 2,300–2,600, and low Ga/Al × 10,000 ratios of 2–4. Eby (1992) proposed that A-type granites can be divided into A_1 and A_2 sub-types based on their tectonic affiliations. The A_1 type granites exhibit low Y/Nb and Yb/Ta ratios, and they maintain a consistent relationship with silica-undersaturated to silica-saturated mafic rocks. Generally, this sub-type forms in intra-plate or rift-related settings, with magma believed to be derived from OIB-like sources. Conversely, the A_2 type granites exhibit high Y/Nb and Yb/Ta ratios and are formed by the partial melting of continental crust within a post-collisional setting. Notably, the A_1 type granites can also form in an extensional setting induced by post-orogenic collapse (Azer, 2006; Xiao et al., 2007; Wang, 2009).

The early Jurassic A-type granites from the Baoji batholith are related to coeval monzodiorites and mafic enclaves (Gong et al., 2021), and exhibit OIB-like trace element features, such as relatively high Nb (45.4×10^{-6}–116.0×10^{-6}) and Y (18.1×10^{-6}–32.0×10^{-6}) contents and low Ta (2.46×10^{-6}–7.27×10^{-6}) and Yb (2.17×10^{-6}–3.39×10^{-6}) contents, with Y/Nb ratios of 0.25–0.46 (average = 0.34) and Yb/Ta ratios of 0.47–0.91 (average = 0.65). In the discrimination diagram by Eby (1992), the K-feldspar granite samples from this study plot fall within or near the A_1 type granite field (Figures 12A–C). However, the discrimination diagram by Hong et al. (1996) demonstrates that the sample plots fall within the fields of 'AA' and 'PA' type granites (Figure 12D). Additionally, all these samples were plotted in the 'within-plate granite' field in the diagrams by Pearce et al. (1984) (Figure 13). Therefore, it appears that ca.188 Ma magmatism may correspond to a post-orogenic collapse or an intraplate extensional setting.

The early Mesozoic granitic rocks are widely distributed in QOB, especially in the west of Danfeng County, Shaanxi Province (Figure 1B). Over the past decades, several studies have demonstrated that these granitoids dated ca. 200–250 Ma can be divided into distinct groups based on different U-Pb ages, geochemical signatures, and petrographic features (Sun et al., 2002; Dong et al., 2012; Wang et al., 2013; 2015). To better understand the early Jurassic tectonic framework of QOB, we collected previously published zircon U-Pb ages of the early Mesozoic granitoids. The available geochronological data demonstrates that the formation of these Triassic granitoids occurred in two major phases: ca. 238–251 and ca. 198–225 Ma (Figure 14A). The first phase granitoids (granitoids I, ca. 238–251 Ma) are primarily exposed in the western Qinling. These rocks are metaluminous to peraluminous and belong to the calc-alkaline to high-K calc-alkaline series, featuring evolved Sr-Nd isotopic compositions (*I*sr

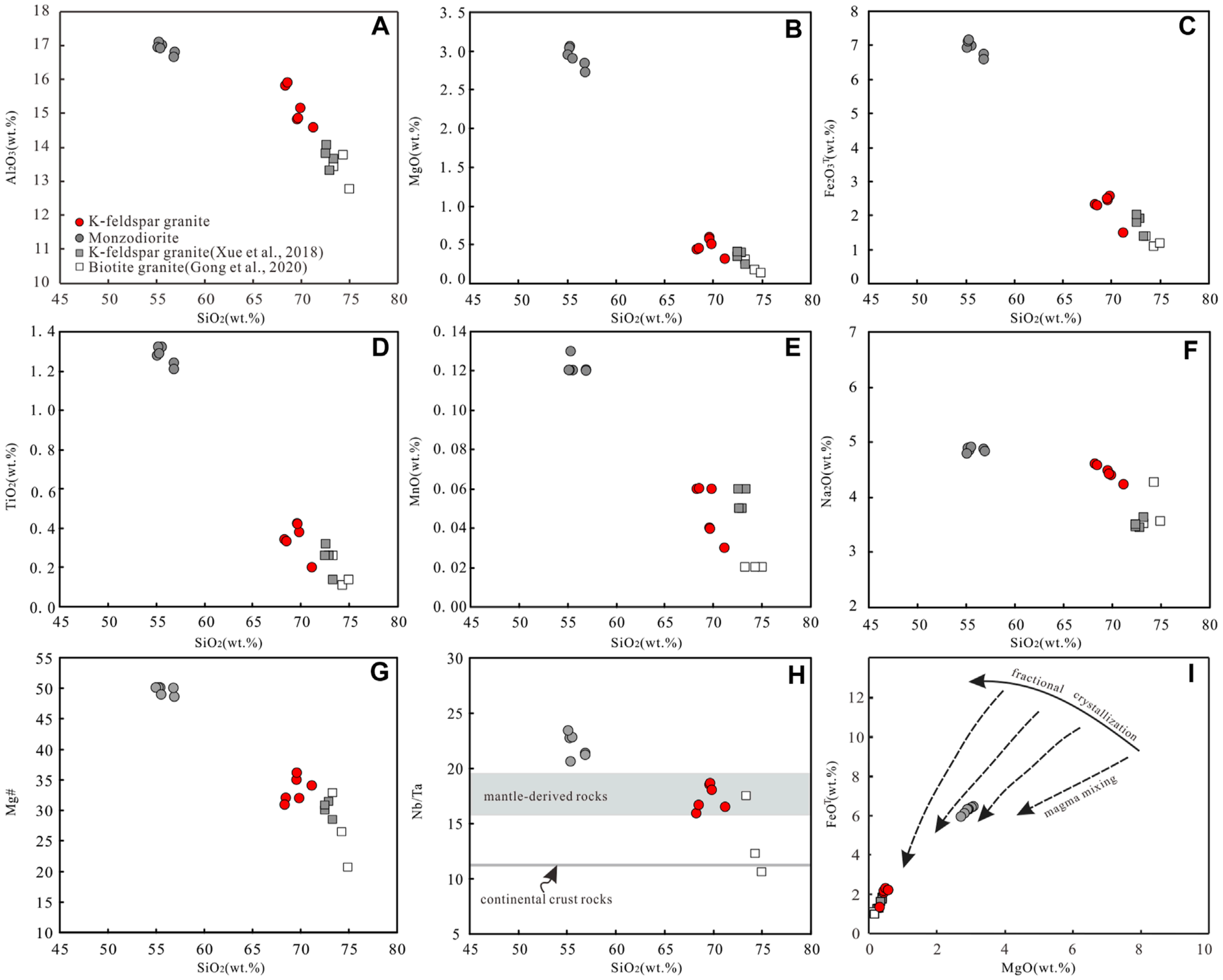

FIGURE 11
Plots of SiO_2 versus **(A)** Al_2O_3, **(B)** MgO, **(C)** $Fe_2O_3{}^T$, **(D)** TiO_2, **(E)** MnO, **(F)** Na_2O, **(G)** Mg#, **(H)** Nb/Ta, and **(I)** MgO versus FeO^T for the for the K-feldspar granite and monzodiorite from the Baoji batholith.

ratios of 0.70727–0.70789 and $\varepsilon_{Nd}(t)$ of −8.51 to −6.77, Zhang et al., 2006). Some of these rocks exhibit geochemical signatures similar to those of adakites derived from over-thickened lower crust (>45 km, Jin et al., 2005), indicating magma generation by partial melting of thickened continental crust, with no involvements of mantle materials (Jin et al., 2005; Zhang et al., 2008). These features resemble syn-collisional magmatism (Song et al., 2015). The second phase of granitoids (granitoids II, ca. 198–225 Ma) widely occur in different tectonic units of QOB. They are metaluminous to peraluminous and primarily belong to the high-K calc-alkaline series (Wang et al., 2013, and references therein). These intrusions are oval or irregular and contain abundant coeval MMEs. Most of these intrusions are composed of I-type granites, as indicated by their evolved Sr-Nd isotopic compositions ($\varepsilon_{Nd}(t)$ = −11.5 to 0.1, Qin et al., 2008; Wang et al., 2011, Wang et al., 2013; Xue et al., 2018) and variable $\varepsilon_{Hf}(t)$ values (−28 to 10) (Figure 6). The MMEs within these granites exhibit variable $\varepsilon_{Hf}(t)$ values (Figure 6), with certain negative $\varepsilon_{Nd}(t)$ values (−7.0 to −3.2). These MMEs are enriched in LILEs and LREE and depleted in HFSEs (Qin et al., 2008; Qin et al., 2009; Qin et al., 2010a; Qin et al., 2010b). The granitic magma was considered to be formed by partial melting of old continental crust, with subsequent mixing of mafic magma derived from the depleted mantle, or the enriched sub-continental lithospheric mantle (Qin et al., 2010a; Qin et al., 2010b). Given the presence of bimodal magmatism indicated by rapakivi-textured granitoids and associated coeval mafic minette dykes (Zhang et al., 2005; Wang et al., 2007; Wang et al., 2011), mantle-derived magmas have significantly contributed in the formation of these granitoids. Therefore, the extensive magmatism during the second phase was interpreted to be associated with lithospheric delamination and asthenosphere upwelling (Zhang et al., 2008; Gong et al., 2009a; Gong et al., 2009b; Zhu et al., 2009) in a post-collisional setting.

There is a gap of ca. 10 Ma between the formation of granitoids II and ca. 188 Ma (Figure 14A). The early Jurassic granitoids are scattered along QOB, contrasting with the intensive magmatism observed in the second stage. Previous studies have also indicated

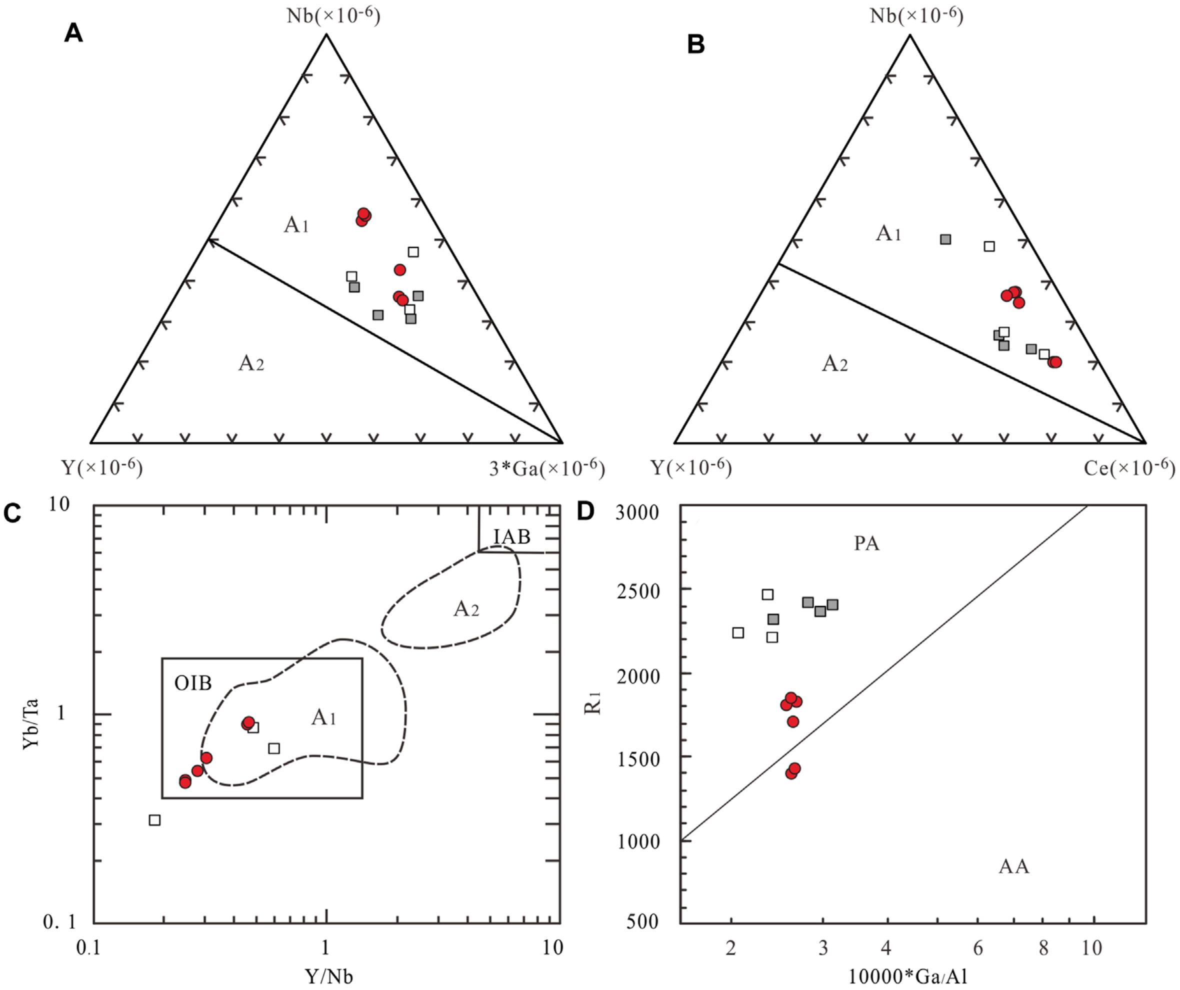

FIGURE 12
Discrimination diagrams for the Yanjiahe K-feldspar granite. **(A–C)** after Eby, 1992; **(D)** after Hong et al., 1996, R_1=4 ∗ Si-11 ∗ (Na+K)-2 ∗ (Fe+Ti).

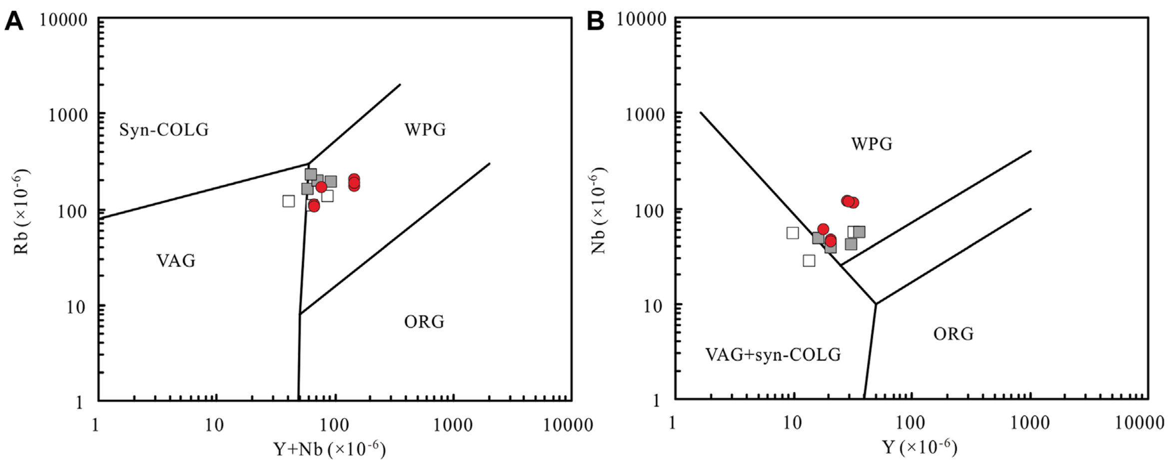

FIGURE 13
Tectonic discrimination diagrams of Rb *versus* Y+Nb **(A)** and Nb *versus* Y **(B)** for the Yanjiahe K-feldspar granite (after Pearce et al., 1984).

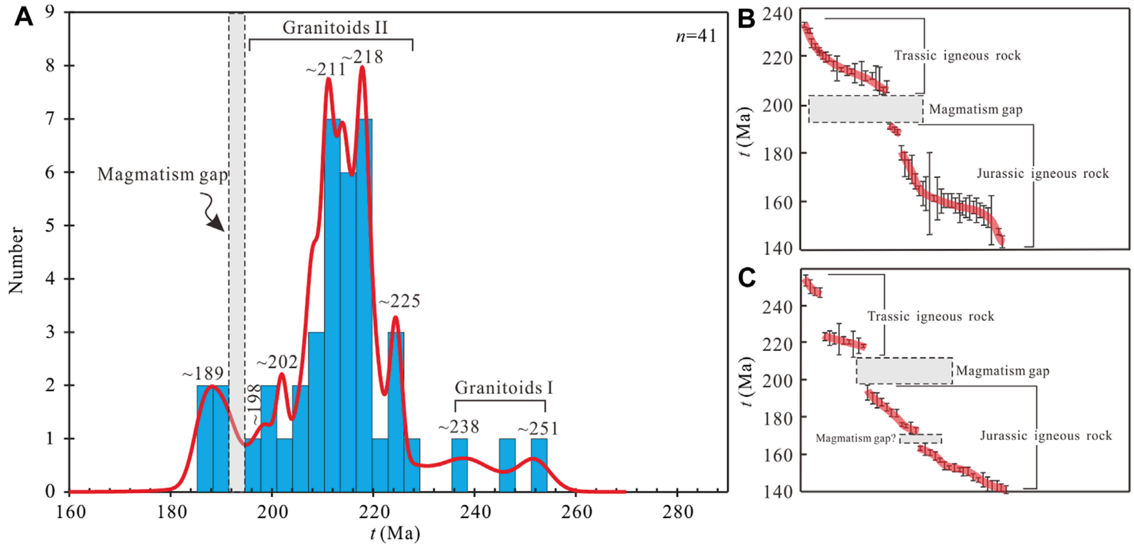

FIGURE 14
Histograms and probability density of zircon U-Pb ages of the Mesozoic granitoids in the QOB **(A)**. Data are from Wang et al., 2013 and references therein; Zhang et al., 2015; Xue et al., 2018; Gong et al., 2021 and this study. Scatter plots of the geochronological data of the Mesozoic intrusions from the Jiao-Liao Massif and the Luxi-Xuhuai regions **(B)**, and from the Yanshan-Liaoxi belt **(C)**. Figure b and c are modified after Zhang et al., 2007.

the involvement of mantle-derived magma in their formation (Li et al., 2010; Dong et al., 2012; Zhang et al., 2015). This implies a gradual reduction of magmatism in QOB since ca. 200 Ma. However, the underplating of mantle-derived magma may induce granitic magmatism.

Mao et al. (2005) compiled previously published age data of Mesozoic metallogenesis in North China and proposed a metallogenic pulse between 160 and 190 Ma in the western Qinling, the northern margin of North China and the southern part of the Great Xing'an Mountains. Among them, the gold deposits in the western Qinling are situated within the interior of strike-slip faults, or on the margin of fault basins. The mineralization is associated with the magmatic-hydrothermal activity induced by local extensions of the thickened lithosphere. Zhang et al. (2007) observed a magmatism gap (191–205 Ma) during the late Triassic-early Jurassic in NCB (Figures 14B,C), and referred to it as the last stage of collision and intracontinental subduction between NCB and SCB. Subsequently, large-scale mantle-derived magma emplacement and mafic-felsic volcanism occurred on either sides of the Yanshan-Liaoxi tectonic belt and the Tan-Lu fault at 180–195 Ma and 175–190 Ma, respectively. Concurrently, normal faulting and rifting occurred along the Yinshan-Yanshan tectonic belt, resulting in a series of extensional basins (Dong et al., 2007; Zhang et al., 2007).

The early Jurassic ca.190 Ma magmatic-metallogenic events in QOB are significantly comparable to that of the early Jurassic magmatism (175–190 Ma) in NCB. Additionally, the occurrence of early Jurassic and late Triassic-early Jurassic fault-controlled rift basins in QOB, along with the formation of Jurassic red sandstones and conglomerates that unconformably overlay the pre-Jurassic strata in SQB (Dong et al., 2005; Dong et al., 2012), are also consistent with post-orogenic extensions. Therefore, we propose that the Jurassic granitoids formed in a post-orogenic setting, indicating that the collisional orogenesis between SCB and NCB probably concluded during the early Jurassic.

7 Conclusion

(1) LA-ICP-MS zircon U-Pb dating results revealed the formation of the K-feldspar granite and the monzodiorite within the northeastern part of the Baoji batholith at 188 ± 2 and 186 ± 2 Ma, respectively.
(2) The K-feldspar granite is characterized by enriched SiO_2, K_2O + Na_2O, Rb, Zr, Hf, and Nb. Generally, this granite exhibits an A-type granite affinity with high Nb/Ta and Ga/Al ratios and zircon saturation temperatures (848°C–900 °C). The geochemical and zircon Hf isotopic data indicated that the parental magma of the monzodiorite probably originated from a metasomatized mantle and experienced crust-mantle magmatic mixing or assimilation during emplacement. The formation of K-feldspar granite was significantly influenced by mixing between a monzodioritic magma and a felsic melt derived from the partial melting of ancient continental crust.
(3) The Yanjiahe K-feldspar granite and monzodiorite from QOB indicated the generation of magmatism in a post-orogenic environment, and the collisional orogenesis between SCB and NCB terminated during the early Jurassic.

Data availability statement

The original contributions presented in the study are included in the article/Supplementary Material, further inquiries can be directed to the corresponding author.

Author contributions

XG: Investigation, Software, Writing–original draft. NA: Supervision, Writing–review and editing, Funding acquisition. YC: Resources, Writing–review and editing. XW: Software, Writing–review and editing. HY: Software, Writing–review and editing. XJ: Writing–review and editing. HC: Software, Supervision, Validation, Writing–review and editing.

Funding

The author(s) declare that financial support was received for the research, authorship, and/or publication of this article. This work is supported by the Natural Science Foundation of Xinjiang Uygur Autonomous Region (No. 2022D01C660 and 2021D01C040), Natural Science Foundation of China (No. 42302059), and Tianchi Talent Program of Xinjiang Uygur Autonomous Region (No. 51052300409).

Conflict of interest

The authors declare that the research was conducted in the absence of any commercial or financial relationships that could be construed as a potential conflict of interest.

Publisher's note

Supplementary material

The Supplementary Material for this article can be found online at: https://www.frontiersin.org/articles/10.3389/feart.2024.1428055/full#supplementary-material

References

Ahmed, H. A., Ma, C. Q., Wang, L. X., Palinkas, L. A., Girei, M. B., Zhu, Y. X., et al. (2018). Petrogenesis and tectonic implications of peralkaline A-type granites and syenites from the Suizhou-Zaoyang region, central China. *J. Earth Sci.* 29, 1181–1202. doi:10.1007/s12583-018-0877-2

Albarède, F., Scherer, E. E., Blichert-Toft, J., Rosing, M., Sirnionovici, A., and Bizzarro, M. (2006). γ-ray irradiation in the early solar system and the conundrum of the ^{176}Lu decay constant. *Geochim. Cosmochim. Acta* 70, 1261–1270. doi:10.1016/j.gca.2005.09.027

Aulbach, S., O'Reilly, S. Y., Griffin, W. L., and Pearson, N. J. (2008). Subcontinental lithospheric mantle origin of high niobium/tantalum ratios in eclogites. *Nat. Geosci.* 1, 468–472. doi:10.1038/ngeo226

Azer, M. K. (2006). The petrogenesis of late Precambrian felsic alkaline magmatism in South Sinai, Egypt. *Acta Geol. Pol.* 56, 463–484.

Bao, Z. A., Chen, L., Zong, C. L., Yuan, H. L., Chen, K. Y., and Dai, M. N. (2017). Development of pressed sulfide powder tablets for *in situ* sulfur and lead isotope measurement using LA-MC-ICP-MS. *Int. J. Mass Spectrom.* 421, 255–262. doi:10.1016/j.ijms.2017.07.015

Bea, F., Arzamastsev, A., Montero, P., and Arzamastseva, L. (2001). Anomalous alkaline rocks of Soustov. Kola: evidence of mantle-derived metasomatic fluids affecting crustal materials. *Contrib. Mineral. Petrol.* 140, 554–566. doi:10.1007/s004100000211

Beard, J. S., and Lofgren, G. E. (1991). Dehydration melting and water-saturated melting of basaltic and andesitic greenstones and amphibolites at 1, 3, and 6.9 kb. *J. Petrol.* 32, 365–401. doi:10.1093/petrology/32.2.365

Blichert-Toft, J., and Albarède, F. (1997). The Lu-Hf isotope geochemistry of chondrites and the evolution of the mantle-crust system. *Earth Planet. Sci. Lett.* 148, 243–258. doi:10.1016/s0012-821x(97)00040-x

Bonin, B. (2007). A-type granites and related rocks: evolution of a concept, problems and prospects. *lithos* 97, 1–29. doi:10.1016/j.lithos.2006.12.007

Buck, W. R. (1991). Modes of continental lithospheric extension. *J. Geophys. Res. Solid Earth Planets* 96, 20161–20178. doi:10.1029/91jb01485

Chappell, B. W., White, A. J. R., Williams, I. S., and Wyborn, D. (2004). Low- and high-temperature granites. *Earth Environ. Sci. Trans. R. Soc. Edinb.* 95, 125–140. doi:10.1017/s0263593300000973

Chappell, B. W., White, A. J. R., Williams, I. S., Wyborn, D., and Wyborn, L. A. I. (2000). Lachlan Fold Belt granites revisited: high and low-temperature granites and their implications. *Aust. J. Earth Sci.* 47, 123–138. doi:10.1046/j.1440-0952.2000.00766.x

Clemens, J. D., Holloway, J. R., and White, A. J. R. (1986). Origin of an A-type granite: experimental constraints. *Am. Mineral.* 71, 317–324.

Collins, W. J., Beams, S. D., White, A. J. R., and Chappell, B. W. (1982). Nature and origin of A-type granites with particular reference to southeastern Australia. *Contrib. Mineral. Petrol.* 80, 189–200.

Conceição, R. V., and Green, D. H. (2004). Derivation of potassic (shoshonitic) magmas by decompression melting of phlogopite+pargasite lherzolite. *lithos* 72, 209–229. doi:10.1016/j.lithos.2003.09.003

Diwu, C. R., Sun, Y., Liu, L., Zhang, C. L., and Wang, H. L. (2010). The disintegration of Kuanping Group in North Qinling Orogenic Belts and Neoproterozoic N-MORB. *Acta Petrol. Sin.* 26, 2025–2038.

Diwu, C. R., Sun, Y., Zhao, Y., Liu, B. X., and Lai, S. C. (2014). Geochronological, geochemical, and Nd-Hf isotopic studies of the Qinling Complex, central China: implications for the evolutionary history of the North Qinling Orogenic Belt. *Geosci. Front.* 5, 499–513. doi:10.1016/j.gsf.2014.04.001

Dong, S. W., Hu, J. M., Li, S. Z., Shi, W., Gao, R., Liu, X. C., et al. (2005). The Jurassic deformation in the Dabashan Mountains and its tectonic significances. *Acta Petrol. Sin.* 21, 1189–1194.

Dong, Y. P., Liu, X. M., Zhang, G. W., Chen, Q., Zhang, X. N., Li, W., et al. (2012). Triassic diorites and granitoids in the Foping area: constraints on the conversion from subduction to collision in the Qinling orogen, China. *J. Asian Earth Sci.* 47, 123–142. doi:10.1016/j.jseaes.2011.06.005

Dong, Y. P., and Santosh, M. (2016). Tectonic architecture and multiple orogeny of the Qinling Orogenic Belt, Central China. *Gondwana Res.* 29, 1–40. doi:10.1016/j.gr.2015.06.009

Dong, Y. P., Zhang, G. W., Neubauer, F., Liu, X. M., Genser, J., and Hauzenberger, C. (2011). Tectonic evolution of the Qinling orogen, China: review and synthesis. *J. Asian Earth Sci.* 41, 213–237. doi:10.1016/j.jseaes.2011.03.002

Dong, S. W., Zhang, Y. Q., Long, C. X., Yang, Z. Y., Ji, Q., Wang, T., et al. (2007). Jurassic tectonic revolution in China and new interpretation of the Yanshan Movement. *Acta Geol. Sin.* 81, 1449–1461.

Eby, G. N. (1990). The A-type granitoids: a review of their occurrence and chemical characteristics and speculations on their petrogenesis. *lithos* 26, 115–134. doi:10.1016/0024-4937(90)90043-z

Eby, G. N. (1992). Chemical subdivision of the A-type granitoids: petrogenetic and tectonic implications. *geology* 20, 641–644. doi:10.1130/0091-7613(1992)020<0641:csotat>2.3.co;2

Elliott, T., Plank, T., Zindler, A., White, W., and Bourdon, B. (1997). Element transport from slab to volcanic front at the Mariana arc. *J. Geophys. Res.* 102, 14991–15019. doi:10.1029/97jb00788

Frost, C. D., and Frost, B. R. (1997). Reduced rapakivi-type granites: the tholeiite connection. *geology* 25, 647–650. doi:10.1130/0091-7613(1997)025<0647:rrtgtt>2.3.co;2

Gao, S., Chen, D. L., Gong, X. K., Ren, Y. F., and Li, H. P. (2015). Zircon U-Pb dating of clastic rocks and granites of Kuanping Group in Dongcha areas of Tianshui, and its geological implications. *Earth Sci. Front.* 22, 255–264. doi:10.13745/j.esf.2015.04.026

Gong, H. J., Zhu, L. M., Sun, B. Y., Li, B., and Guo, B. (2009a). Zircon U-Pb ages and Hf isotope characteristics and their geological significance of the Shahewan, Caoping and Zhashui granitic plutons in the South Qinling orogeny. *Acta Petrol. Sin.* 25, 248–264.

Gong, H. J., Zhu, L. M., Sun, B. Y., Li, B., Guo, B., and Wang, J. Q. (2009b). Zircon U-Pb ages and Hf isotopic composition of the Dongjiangkou granitic pluton and its mafic enclaves in the South Qinling terrain. *Acta Petrol. Sin.* 25, 3029–3042.

Gong, X. K., Cai, H. M., Guo, R. Q., Liu, G. P., Tan, J., and Maihesuti, M. (2021). Early jurassic A-type granites in the western North Qinling orogen, central China, and its geological significance. *Chin. J. Geol.* 56, 158–181. doi:10.12017/dzkx.2021.011

Gong, X. K., Chen, D. L., Ren, Y. F., Liu, L., Gao, S., and Yang, S. J. (2016). Identification of coesite-bearing amphibolite in the North Qinling and its geological significance. *Chin. Sci. Bull.* 61, 1365–1378. doi:10.1360/n972015-01277

Green, T. H. (1995). Significance of Nb/Ta as an indicator of geochemical processes in the crust-mantle system. *Chem. Geol.* 120, 347–359. doi:10.1016/0009-2541(94)00145-x

Griffin, W. L., Pearson, N. J., Belousova, E., Jackson, S. E., van Achterbergh, E., O'Reilly, S. Y., et al. (2000). The Hf isotope composition of cratonic mantle: LAM-MC-ICPMS analysis of zircon megacrysts in kimberlites. *Geochim. Cosmochim. Acta* 64, 133–147. doi:10.1016/s0016-7037(99)00343-9

Hofmann, A. W. (1988). Chemical differentiation of the Earth: the relationship between mantle, continental crust, and oceanic crust. *Earth Planet. Sci. Lett.* 90, 297–314. doi:10.1016/0012-821x(88)90132-x

Hong, D. W., Wang, S. G., Han, B. F., and Jin, M. Y. (1996). Post-orogenic alkaline granites from China and comparisons with anorogenic alkaline granites elsewhere. *J. Southeast Asian Earth Sci.* 13, 13–27. doi:10.1016/0743-9547(96)00002-5

Jin, W. J., Zhang, Q., He, D. F., and Jia, X. Q. (2005). SHRIMP dating of adakites in western Qinling and their implications. *Acta Petrol. Sin.* 21, 959–966.

King, P. L., White, A. J. R., Chappell, B. W., and Allen, C. M. (1997). Characterization and origin of aluminous A-type granites from the Lachlan Fold Belt, southeastern Australia. *J. Petrol.* 38, 371–391. doi:10.1093/petroj/38.3.371

Li, L., Zhang, C. L., Zhou, Y., Tian, H. Q., and Li, X. F. (2012). Early Mesozoic crust- and mantle-derived magmatic mixing in the Qinling Orogeny: evidence from geochemistry of mafic microgranular enclaves in the Dongjiangkou pluton. *Geol. J. China Univ.* 18, 291–306.

Li, S. Q., Yang, X. Y., Qu, W. J., Chen, F. K., and Sun, W. D. (2010). Molybdenite Re-Os age and metallogeny of the Yueheping skarn molybdenum deposit in Ningshan, southern Qinling. *Acta Petrol. Sin.* 26, 1479–1486.

Li, Y., Yang, J. S., Dilek, Y., Zhang, J., Pei, X. Z., Chen, S. Y., et al. (2015). Crustal architecture of the Shangdan suture zone in the early Paleozoic Qinling orogenic belt, China: record of subduction initiation and back-arc basin development. *Gondwana Res.* 27, 733–744. doi:10.1016/j.gr.2014.03.006

Liégeois, J. P. (1998). Some words on the post-collisional magmatism. *Lithos* 45, 15–18.

Liu, L., Liao, X. Y., Wang, Y. W., Wang, C., Santosh, M., Yang, M., et al. (2016). Early Paleozoic tectonic evolution of the North Qinling Orogenic Belt in Central China: insights on continental deep subduction and multiphase exhumation. *Earth-Sci. Rev.* 159, 58–81. doi:10.1016/j.earscirev.2016.05.005

Loiselle, M. C., and Wones, D. R. (1979). Characteristics and origin of anorogenic granites. *Abstr. Pap. be Present. A. T. Annu. Meet. Geol. Soc. Am. Assoc. Soc.* 11, 468. San Diego, California.

Ludwig, K. R. (2003). ISOPLOT 3.0: a geochronological toolkit for microsoft excel. *Berkeley Geochronol. Cent. Spec. Publ.* No. 4.

Maniar, P. D., and Piccoli, P. M. (1989). Tectonic discrimination of granitoids. *Geol. Soc. Am. Bull.* 101, 635–643. doi:10.1130/0016-7606(1989)101<0635:tdog>2.3.co;2

Mao, J. W., Xie, G. Q, Zhang, Z. H., Li, X.F., Wang, Y. T., and Zhang, C. Q. (2005). Mesozoic large-scale metallogenic pulses in North China and corresponding geodynamic settings. *Acta Petrol. Sin.* 21, 169–188.

Mattauer, M., Matte, P., Malavieille, J., Tapponnier, P., Maluski, H., Xu, Z. Q., et al. (1985). Tectonics of the qinling belt: build-up and evolution of eastern asia. *Nature* 317, 496–500. doi:10.1038/317496a0

McDonough, W. F., and Sun, S. S. (1995). The composition of the earth. *Chem. Geol.* 120, 223–253. doi:10.1016/0009-2541(94)00140-4

Niu, Y. L., and O'Hara, M. J. (2009). MORB mantle hosts the missing Eu (Sr, Nb, Ta and Ti) in the continental crust: new perspectives on crustal growth, crust-mantle differentiation and chemical structure of oceanic upper mantle. *lithos* 112, 1–17. doi:10.1016/j.lithos.2008.12.009

Patiño Douce, A. E. (1997). Generation of metaluminous A-type granites by low-pressure melting of calc-alkaline granitoids. *geology* 25, 743–746. doi:10.1130/0091-7613(1997)025<0743:gomatg>2.3.co;2

Pearce, J. A., Harris, N. B. W., and Tindle, A. G. (1984). Trace element discrimination diagrams for the tectonic interpretation of granitic rocks. *J. Petrol.* 25, 956–983. doi:10.1093/petrology/25.4.956

Pearce, J. A., and Peate, D. W. (1995). Tectonic implications of the composition of volcanic arc magmas. *Annu. Rev. Earth Planet. Sci.* 23, 251–285. doi:10.1146/annurev.earth.23.1.251

Qin, J. F., Lai, S. C., Diwu, C. R., Ju, Y. J., and Li, Y. F. (2010b). Magma mixing origin for the post-collisional adakitic monzogranite of the Triassic Yangba pluton, Northwestern margin of the South China block: geochemistry, Sr-Nd isotopic, zircon U-Pb dating and Hf isotopic evidences. *Contrib. Mineral. Petrol.* 159, 389–409. doi:10.1007/s00410-009-0433-2

Qin, J. F., Lai, S. C., Grapes, R., Diwu, C. R., Ju, Y. J., and Li, Y. F. (2009). Geochemical evidence for origin of magma mixing for the Triassic monzonitic granite and its enclaves at Mishuling in the Qinling orogen (central China). *lithos* 112, 259–276. doi:10.1016/j.lithos.2009.03.007

Qin, J. F., Lai, S. C., Grapes, R., Diwu, C. R., Ju, Y. J., and Li, Y. F. (2010a). Origin of Late Triassic high-Mg adakitic granitoid rocks from the Dongjiangkou area, Qinling orogen, central China: implications for subduction of continental crust. *lithos* 120, 347–367. doi:10.1016/j.lithos.2010.08.022

Qin, J. F., Lai, S. C., and Li, Y. F. (2005). Petrogenesis and geological significance of Yangba granodiorites from Bikou area, northern margin of Yangtze Plate. *Acta Petrol. Sin.* 21, 697–710.

Qin, J. F., Lai, S. C., Wang, J., and Li, Y. F. (2008). Zircon LA-ICP-MS U-Pb age, Sr-Nd-Pb isotopic compositions and geochemistry of the Triassic post-collisional Wulong adakitic granodiorite in the South Qinling, Central China, and its petrogenesis. *Acta Geol. Sin. Engl. Ed.* 82, 425–437. doi:10.1111/j.1755-6724.2008.tb00593.x

Qiu, J. S., Wang, D. Z., Satoshi, K., and Brent, I. A. M. (2000). Geochemistry and petrogenesis of aluminous A-type granites in the coastal area of Fujian Province. *geochimica* 29, 313–321. doi:10.19700/j.0379-1726.2000.04.001

Rapp, R. P., and Watson, E. B. (1995). Dehydration melting of metabasalt at 8-32 kbar: implications for continental growth and crust-mantle recycling. *J. Petrol.* 36, 891–931. doi:10.1093/petrology/36.4.891

Ratschbacher, L., Hacker, B. R., Calvert, A., Webb, L. E., Crimmer, J. C., McWilliams, M. O., et al. (2003). Tectonics of the Qinling (Central China): tectonostratigraphy, geochronology, and deformation history. *Tectonophysics* 366, 1–53. doi:10.1016/s0040-1951(03)00053-2

Rollinson, H. (1993). *Using geochemical data: evaluation, presentation, interpretation*. London: Longman Scientific & Technical, 1–384.

Rudnick, R. L., and Gao, S. (2003). *Composition of the continental crust*. Editor H. D. Holland, and K. K. Turekian, K.K (Oxford: Treatise on Geochemistry, Elsevier–Pergamon), 1–64.

Shaw, S. E., and Flood, R. H. (2009). Zircon Hf isotopic evidence for mixing of crustal and silicic mantle-derived magmas in a zoned granite pluton, eastern Australia. *J. Petrol.* 50, 147–168. doi:10.1093/petrology/egn078

Shellnutt, J. G., and Zhou, M. F. (2007). Permian peralkaline, peraluminous and metaluminous A-type granites in the Panxi district, SW China: their relationship to the Emeishan mantle plume. *Chem. Geol.* 243, 286–316. doi:10.1016/j.chemgeo.2007.05.022

Song, S. G., Wang, M. J., Wang, C., and Niu, Y. L. (2015). Magmatism during continental collision, subduction, exhumation and mountain collapse in collisional orogenic belts and continental net growth: a perspective. *Sci. China Earth Sci.* 58, 1284–1304. doi:10.1007/s11430-015-5102-x

Song, Y. H., Hao, L. B., Yang, F. C., Zhao, D. F., and Zhang, Z. H. (2021). Early Cretaceous A-type granites in the Dandong area, NE China and its geodynamical implications. *Acta Geol. Sin. Engl. Ed.* 95, 1472–1482. doi:10.1111/1755-6724.14499

Sun, S. S., and McDonough, W. F. (1989). Chemical and isotopic systematics of oceanic basalts: implications for mantle composition and processes. *Spec. Publ. - Geol. Soc. Lond.* 42, 313–345. doi:10.1144/gsl.sp.1989.042.01.19

Sun, W. D., Li, S. G., Chen, Y. D., and Li, Y. J. (2002). Timing of synorogenic granitoids in the South Qinling, central China: constraints on the evolution of the Qinling-Dabie orogenic belt. *J. Geol.* 110, 457–468. doi:10.1086/340632

Sun, Y., Liu, X. X., Han, S., and Zhang, G. W. (1996). Composition and formation of Palaeozoic Erlangping ophiolitic slab, North Qinling: evidence from geology and geochemistry. *Sci. China Earth Sci.* 39, 50–59.

Wang, X. R., Hua, H., and Sun, Y. (1995). A Study on Microfossils of the Erlangping Group in Wantan Area Xixia County, Henan Province. *J. Northwest Univ. Nat. Sci. Ed.* 25, 353–358.

Wang, F., Lu, X. X., Lo, C. H., Wu, F. Y., He, H. Y., Yang, L. K., et al. (2007). Post-collisional, potassic monzonite-minette complex (Shahewan) in the Qinling Mountains (central China): $^{40}Ar/^{39}Ar$ thermochronology, petrogenesis, and implications for the dynamic setting of the Qinling orogeny. *J. Asian Earth Sci.* 31, 153–166. doi:10.1016/j.jseaes.2007.06.002

Wang, H., Wu, Y. B., Gao, S., Zheng, J. P., Liu, Q., Liu, X. C., et al. (2014). Deep subduction of continental crust in accretionary orogen: evidence from U-Pb dating on diamond-bearing zircons from the Qinling Orogen, central China. *lithos* 190-191, 420–429. doi:10.1016/j.lithos.2013.12.021

Wang, X. X., Wang, T., Castro, A., Pedreira, R., Lu, X. X., and Xiao, Q. H. (2011). Triassic granitoids of the Qinling orogen, central China: genetic relationship of enclaves and rapakivi-textured rocks. *lithos* 126 (3-4), 369–387. doi:10.1016/j.lithos.2011.07.007

Wang, X. X., Wang, T., and Zhang, C. L. (2013). Neoproterozoic, paleozoic, and mesozoic granitoid magmatism in the Qinling Orogen, China: constraints on orogenic process. *J. Asian Earth Sci.* 72, 129–151. doi:10.1016/j.jseaes.2012.11.037

Wang, X. X., Wang, T., and Zhang, C. L. (2015). Granitoid magmatism in the Qinling orogen, central China and its bearing on orogenic evolution. *Sci. China Earth Sci.* 58, 1497–1512. doi:10.1007/s11430-015-5150-2

Wang, Y. (2009). Geochemistry of the Baicha A-type granite in Beijing Municipality: petrogenetic and tectonic implications. *Acta Petrol. Sin.* 25, 13–24.

Watson, E. B., and Harrison, T. M. (1983). Zircon saturation revisited: temperature and composition effects in a variety of crustal magma types. *Earth Planet. Sci. Lett.* 64, 295–304. doi:10.1016/0012-821x(83)90211-x

Whalen, J. B., Currie, K. L., and Chappell, B. W. (1987). A-type granites: geochemical characteristics, discrimination and petrogenesis. *Contrib. Mineral. Petrol.* 95, 407–419. doi:10.1007/bf00402202

Willett, S., Beaumont, C., and Fullsack, P. (1993). Mechanical model for the tectonics of doubly vergent compressional orogens. *Geology* 21, 371–374.

Wu, F. Y., Li, X. H., Yang, J. H., and Zheng, Y. F. (2007). Discussions on the petrogenesis of granites. *Acta Petrol. Sin.* 23, 1217–1238.

Wu, F. Y., Sun, D. Y., Li, H. M., Jahn, B. M., and Wilde, S. (2002). A-type granites in northeastern China: age and geochemical constraints on their petrogenesis. *Chem. Geol.* 187, 143–173. doi:10.1016/s0009-2541(02)00018-9

Wu, Y. B., and Zheng, Y. F. (2013). Tectonic evolution of a composite collision orogen: an overview on the Qinling-Tongbai-Hong'an-Dabie-Sulu orogenic belt in central China. *Gondwana Res.* 23, 1402–1428. doi:10.1016/j.gr.2012.09.007

Xiao, E., Qiu, J. S., Xu, X. S., Jiang, S. Y., Hu, J., and Li, Z. (2007). Geochronology and geochemistry of the Yaokeng alkaline granitic pluton in Zhejiang Province: petrogenetic and tectonic implications. *Acta Petrol. Sin.* 23, 1431–1440.

Xue, Y. Y., Siebel, W., He, J. F., Zhang, H., and Chen, F. K. (2018). Granitoid petrogenesis and tectonic implications of the late Triassic Baoji pluton, north Qinling Orogen, China: zircon U-Pb ages and geochemical and Sr-Nd-Pb-Hf isotopic compositions. *J. Geol.* 126, 119–139. doi:10.1086/694765

Yan, Q. R., Wang, Z. Q., Chen, J. L., Yan, Z., Wang, T., Liu, Q. G., et al. (2007). Tectonic setting and SHRIMP age of volcanic rocks in the Xieyuguan and Caotangou Groups:implications for the North Qinling Orogenic Belt. *Acta Petrol. Sin.* 81, 488–500.

Yang, J. H., Wu, F. Y., Chung, S. L., Wilde, S. A., and Chu, M. F. (2006). A hybrid origin for the Qianshan A-type granite, northeast China: geochemical and Sr-Nd-Hf isotopic evidence. *lithos* 89, 89–106. doi:10.1016/j.lithos.2005.10.002

Yang, M., Liu, L., Wang, Y. W., Liao, X. Y., Kang, L., and Gai, Y. S. (2016). Geochronology of detrital zircons from metaclastic of Erlangping complex in the North Qinling belt and its tectonic implication. *Acta Petrol. Sin.* 32, 1452–1466.

Yang, S. J., Chen, D. L., Gong, X. K., and Zhao, J. (2015). The geochemistry, chronology and its geological implications of leucosomes in the basic volcanics of Erlangping Group in eastern segment of the North Qinling. *Acta Petrol. Sin.* 31, 2009–2022.

Yuan, C., Zhou, M. F., Sun, M., Zhao, Y. J., Wilde, S., Long, X. P., et al. (2010). Triassic granitoids in the eastern Songpan Ganzi Fold Belt, SW China: magmatic response to geodynamics of the deep lithosphere. *Earth Planet. Sci. Lett.* 290, 481–492. doi:10.1016/j.epsl.2010.01.005

Yuan, H. L., Gao, S., Dai, M. N., Zong, C. L., Guenther, D., Fontaine, G. H., et al. (2008). Simultaneous determinations of U-Pb age, Hf isotopes and trace element compositions of zircon by excimer laser-ablation quadrupole and multiple-collector ICP-MS. *Chem. Geol.* 247, 100–118. doi:10.1016/j.chemgeo.2007.10.003

Zhang, C. L., Wang, T., and Wang, X. X. (2008). Origin and tectonic setting of the Early Mesozoic granitoids in Qinling orogenic belt. *Geol. J. China Univ.* 14, 304–316.

Zhang, C. L., Zhang, G. W., Yan, Y. X., and Wang, Y. (2005). Origin and dynamic significance of Guangtoushan granitic plutons to the north of Mianlue zone in southern Qinling. *Acta Petrol. Sin.* 21, 711–720.

Zhang, H., Chen, D. L., Zhai, M. G., Zhang, F. X., Gong, X. K., and Sun, W. D. (2015). Molybdenite Re-Os dating and its tectonic significance of the Guilingou porphyry molybdenum deposit, southern Qinling. *Acta Petrol. Sin.* 31, 2023–2037.

Zhang, Q., Ran, H., and Li, C. D. (2012). A-type granite: what is the essence? *Acta Petrol. Mineral.* 31, 621–626.

Zhang, Y. W., Zhang, X. F., Chen, L. X., Pang, Z. S., Chen, H., Xue, J. L., et al. (2023). Geochronology and geochemistry of early cretaceous A-type granites in central-eastern Inner Mongolia, China: implications for late mesozoic tectonic evolution of the southern Great Xing'an Range. *Acta Geol. Sin. Engl. Ed.* 97, 1094–1111. doi:10.1111/1755-6724.15062

Zhang, Z. Q., Zhang, G. W., Liu, D. Y., Wang, Z. Q., Tan, S. H., and Wang, J. H. (2006). *Isotopic geochronology and geochemistry of ophiolites, granites and clastic sedimentary rocks in the Qinling Orogenic Belt*. Beijing: Geological Publishing House, 1–348.

Zhao, J., Chen, D. L., Tan, Q. H., Chen, M., Zhu, X. H., Guo, C. L., et al. (2012). Zircon LA-ICP-MS U-Pb dating of basic volcanics from erlangping group of the North Qinling, eastern Qinling mountains and its geological implications. *Earth Sci. Front.* 19, 118–125.

Zhao, X. F., Zhou, M. F., Li, J. W., and Wu, F. Y. (2008). Association of Neoproterozoic A- and I-type granites in South China: implications for generation of A-type granites in a subduction-related environment. *Chem. Geol.* 257, 1–15. doi:10.1016/j.chemgeo.2008.07.018

Zhao, Z. F., Zheng, Y. F., Wei, C. S., and Wu, F. Y. (2011). Origin of post-collisional magmatic rocks in the Dabie orogen: implications for crust-mantle interaction and crustal architecture. *lithos* 126, 99–114. doi:10.1016/j.lithos.2011.06.010

Zhang, Y. Q., Dong, S. W., Zhao, Y., and Zhang, T. (2007). Jurassic tectonics of North China: A synthetic view. *Acta Geol. Sin.* 81, 1462–1480.

Zhu, L. M., Ding, Z. J., Yao, S. Z., Zhang, G. W., Song, S. G., Qu, W. J., et al. (2009). Ore-forming event and geodynamic setting of molybdenum deposit at Wenquan in Gansu Province, Western Qinling. *Chin. Sci. Bull.* 54, 2309–2324. doi:10.1007/s11434-009-0094-6

Zorpi, M. J., Coulon, C., Orsini, J. B., and Cocirta, C. (1989). Magma mingling, zoning and emplacement in calc-alkaline granitoid plutons. *Tectonophysics* 157, 315–329. doi:10.1016/0040-1951(89)90147-9